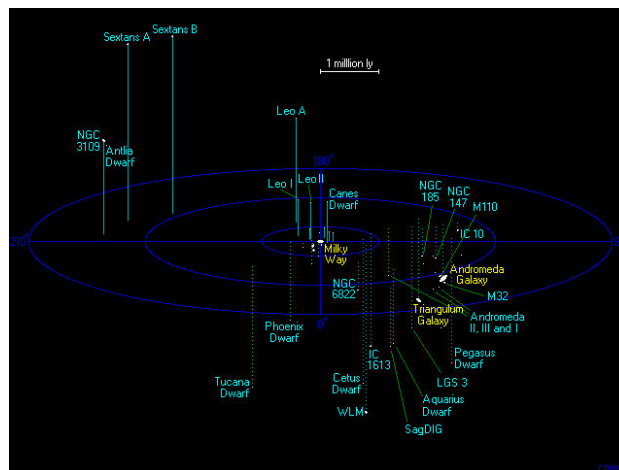


## *HII REGION DETECTION IN LOCAL GROUP CENSUS*



*DIPLOMA THESIS BY  
TREMOU E EVAGELIA*

*SUPERVISOR  
JOHN H SEIRADAKIS*

THESSALONIKI, 2006

*To The Daydreamers...*

## Acknowledgements

After having finished this diploma thesis, I feel urged to express my deep gratitude to those who helped me by all means. In particular, I want to thank Professor Seiradakis John H and Associated Professor Avgouloupis Stavros. Their trust and support deeply touched me and this venture came true. Their immense love for astronomy and the encouragement they gave me seem invaluable. I couldn't fail to express my sincere thanks to my university colleague Mislis Dimitrios, who with his knowledge, patience and infinite fervour for astronomy helped me finish this project. Moreover I would like to express my thanks to the technician of the Observatory of Thessaloniki Tsorlinis Evangelos. Finally, I am grateful to the Isaac Newton Group (ING) for providing us the data.



# Contents

<b>1</b>	<b>Local Group of galaxies</b>	<b>1</b>
1.1	<b>Introduction</b>	1
1.1.1	Irregular galaxies	2
1.1.2	Spectral types of stars	3
1.1.3	H-R	3
1.1.4	HII regions	9
1.1.5	Structure of an HII region	10
1.1.6	Populations of HII regions in irregular galaxies	11
<b>2</b>	<b>Studies in the galaxies IC 10 and Sextan B</b>	<b>15</b>
2.1	<b>Introduction</b>	15
2.1.1	IC 10	15
2.1.2	Sextan B	17
<b>3</b>	<b>Observations and Data reduction</b>	<b>19</b>
3.1	<b>Observations</b>	19
3.2	<b>Data Reduction</b>	24
3.2.1	Image distortion	24
3.2.2	Continuum subtraction	26
3.2.3	Flux calibration	27
3.3	<b>Construction of the HII regions catalogue</b>	31
3.3.1	Hot stars in IC10 and SexB	31
3.4	<b>FOCAS Software</b>	32
3.5	<b>Astrometry</b>	36
<b>4</b>	<b>Results</b>	<b>39</b>
4.1	<b>IC 10 and Sextan B</b>	39



# List of Figures

1.1.1 The Local Group of Galaxies. . . . .	2
1.1.2 Hubble Sequence. . . . .	3
1.1.3 H-R diagram. . . . .	4
1.1.4 H-R Diagram. . . . .	7
1.1.5 M 57 Planetary Nebulae. . . . .	8
1.1.6 Stromgren sphere. . . . .	9
1.1.7 Stratification of the ions within HII regions for different temperatures of their ionizing stars . . . . .	11
2.1.1 IC 10 galaxy. . . . .	16
2.1.2 Sextan B galaxy. . . . .	18
3.1.1 Dome of Isaac Newton Telescope. . . . .	19
3.1.2 Isaac Newton Telescope. . . . .	21
3.1.3 The Wide Field Camera. . . . .	23
3.1.4 The filters R (Harris), H, SII. . . . .	24
3.2.1 The transmission curves of filters g, He, OIII and stY. . . . .	25
3.2.2 The spectrum of Feige 24 and the transmission curve of the Ha filter. . . . .	28
3.3.1 The blue stars in the IC10 galaxy. . . . .	32
3.3.2 Luminosity Function in the IC10 galaxy. . . . .	32
3.3.3 The blue stars in the Sextan B galaxy. . . . .	33
3.3.4 Luminosity Function in the Sextan B galaxy. . . . .	33
4.1.1 IC10. . . . .	41
4.1.2 Color - Color diagram of the IC 10 galaxy. . . . .	41
4.1.3 Color - Color diagram of the Sextan B galaxy. . . . .	42
4.1.4 Luminosities vs Radius of HII regions in IC 10 galaxy. . . . .	42
4.1.5 Luminosities vs Radius of HII regions in Sextan B galaxy. . . . .	43
4.1.6 Sextan B. . . . .	43
4.1.7 Color-Color map of IC 10. . . . .	54



# List of Tables

1.1.1 A schematic plot of the H-R diagram . . . . .	6
2.1.1 Parameters of IC 10 galaxy. . . . .	16
2.1.2 Parameters of Sextan B galaxy. . . . .	18
3.1.1 Optical characteristics of INT. . . . .	22
3.1.2 Information about the observations. . . . .	23
3.2.1 Standard Stars Photometry . . . . .	27
3.2.2 CCDs information . . . . .	28
3.2.3 Fluxes and CF in HX and HV . . . . .	29
3.2.4 Comparison of Fluxes . . . . .	30
3.4.1 Flags in FOCAS . . . . .	36
4.1.1 IC 10 objects . . . . .	44
4.1.2 IC 10 objects . . . . .	45
4.1.3 Sextan B objects . . . . .	46
4.1.4 Sextan B objects . . . . .	47
4.1.5 IC 10 Astrometry . . . . .	48
4.1.6 IC 10 Astrometry . . . . .	49
4.1.7 Sextan B Astrometry . . . . .	50
4.1.8 Temperature and mass of HII regions in IC 10 galaxy . . . . .	51
4.1.9 Temperature and mass of HII regions in IC 10 galaxy . . . . .	52
4.1.10 Temperature and mass of HII regions in Sextan B galaxy . . . . .	53

## Abstract

The present diploma thesis deals with the detection of HII regions in two galaxies. Actually it refers to the IC10 and Sextan B dwarf irregular galaxies, which are part of our Local Group Census of Galaxies. The data reduction, which has been worked out with the astronomical package Image Reduction and Analysis Facility, **IRAF** is analytically below mentioned. The data was taken with the 2.5m Isaac Newton Telescope which is located in La Palma at the Canary islands as well as with the Wide Field Camera. Narrow band and broad band filters were used. The method we used for the data analysis is known as the Hot Stars Method. It is also interesting to note that the study of the physical parameters of HII regions is achieved with the help and the tools of nuclear physics. In summary by using the "Hot Stars Method", in this project we have managed to present the photometric and the astrometric catalogues for these two galaxies.

# Chapter 1

## Local Group of galaxies

### 1.1 Introduction

This is "our" group of galaxies. It was first recognized by Hubble, in the time of the first distance determinations and redshift measurements. The Local Group contains the Andromeda Galaxy (M31) and its satellites M32 and M110, as well as the Triangulum galaxy (M33). Other members (over 30 in all) include our Milky Way Galaxy, the Large and the Small Magellanic Cloud (LMC and SMC), which have been known before the invention of the telescope (as was the Andromeda Galaxy), as well as several smaller galaxies which were discovered more recently. These galaxies are spread in a volume of nearly 10 million light years diameter, centered somewhere between the Milky Way and M31. Membership is not certain for all these galaxies, and there are possible other candidate members. Of the Local Group member galaxies, the Milky Way and M31 are by far the most massive, and therefore dominant members. Each of these two giant spirals has accumulated a system of satellite galaxies, where the system of the Milky Way contains many (nearby) dwarf galaxies, spread all over the sky, namely Sag DEG, LMC, SMC, and the dwarf galaxies in Ursa Minor, Draco, Carina, Sextans (dwarf), Sculptor, Fornax, Leo I and Leo II; and the system of the Andromeda galaxy is seen from outside, and thus grouped around its main galaxy M31 in Andromeda, containing bright nearby M32 and M110 as well as fainter and more far-out NGC 147 and 185, the very faint systems And I, And II, And III, and, possibly, And IV. The third-largest galaxy, the Triangulum spiral M33, may or may not be an outlying gravitationally bound companion of M31, but has itself probably the dwarf LGS 3 as a satellite. The other members cannot be assigned to one of the main subgroups, and float quite alone in the gravitational field of the giant group members. The substructures of the group are probably not stable. Observations and calculations suggest that the group is highly dynamic and has changed significantly in the past: The galaxies around the large elliptical Maffei 1 have probably been once part of our galaxy group. As this shows, the Local Group is not isolated, but in gravitational interaction, and member exchange, with the nearest surrounding groups, notably: the Maffei 1 group, which besides the giant elliptical galaxy Maffei 1 also contains smaller Maffei 2, and is associated with nearby IC 342. This group is highly obscured by dark dust near the Milky Way's equatorial plane. the Sculptor Group or South Polar Group (with members situated around the South Galactic pole),

## 2CHAPTER 1. *LOCAL GROUP OF GALAXIES*

dominated by NGC 253; the M81 group; and the M83 group. In the future, interaction between the member galaxies and with the cosmic neighborhood will continue to change the Local Group. Some astronomers speculate that the two large spirals, our Milky Way and the Andromeda Galaxy, may perhaps collide and merge in some distant future, to form a giant elliptical. In addition, there is evidence that our nearest big cluster of galaxies, the Virgo Cluster, will probably stop our cosmological recession away from it, accelerate the Local Group toward itself so that it will finally fall and merge into this huge cluster of galaxies.

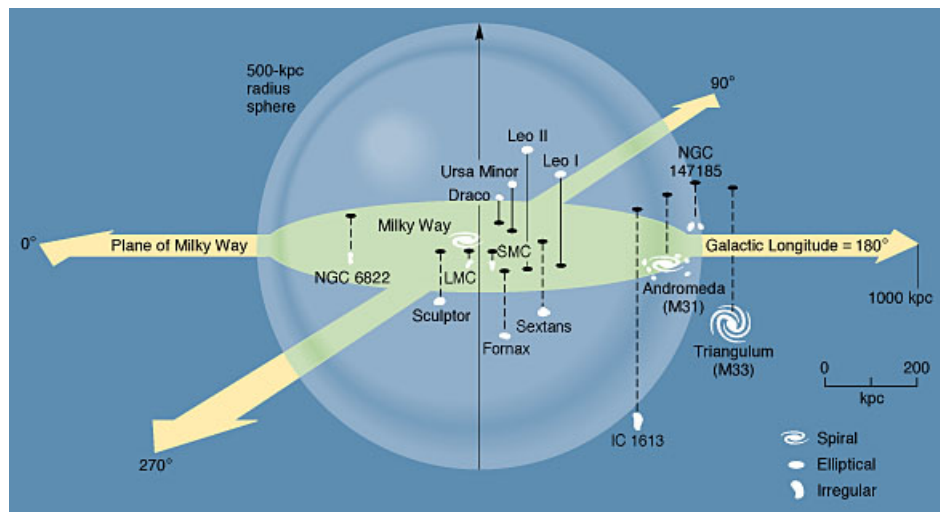


Figure 1.1.1: The Local Group of Galaxies.

### 1.1.1 Irregular galaxies

Irregular galaxies are just that: irregular. They do not fit into the spiral/elliptical classification scheme Hubble developed, nor do they show distinctive features as a class. They are generally just a conglomeration of galaxies which are united only by the fact that they don't belong anywhere else. Irregular galaxies have a chaotic appearance, with large clouds of gas and dust mixed with both old and young stars at random. Some are undergoing a burst of star formation now, so many H II regions are seen in them. Others have very little star formation going on in them (even some of those with a lot of gas and dust still in them). They have no apparent spiral arms or nuclear bulge. Irregulars are generally faint. They make up probably about 25% of all galaxies. Irregular galaxies are divided into two groups. Type Irr I galaxies can be resolved into nebulae, stars, and clusters; type Irr II galaxies cannot be resolved into these components. Other than this classification, irregular galaxies can have pretty much any shape they please. The best-studied examples of irregular galaxies are the Large and Small Magellanic clouds (LMC and SMC), which are members of our own cluster of galaxies, called the Local Group.

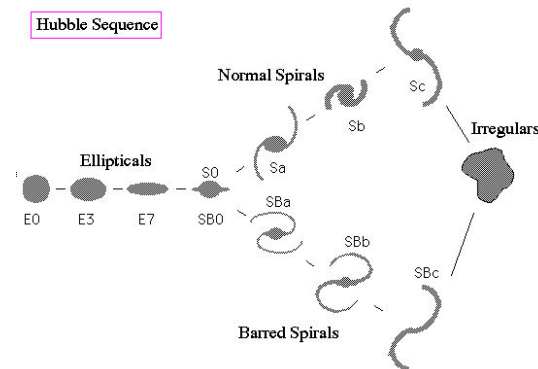


Figure 1.1.2: Hubble Sequence.

### 1.1.2 Spectral types of stars

Stars are divided into a series of spectral types based on the appearance of their absorption spectra. Some stars have a strong signature of hydrogen (O and B stars), others have weak hydrogen lines, but strong lines of calcium and magnesium (G and K stars). After years of cataloging stars, they were divided into 7 basic classes: O, B, A, F, G, K and M. Note that the spectra classes are also divisions of temperature such that O stars are hot, M stars are cool.

Between the classes there were 10 subdivisions numbered 0 to 9. For example, our Sun is a G2 star. Sirius, a hot blue star, is type B3.

Why do some stars have strong lines of Hydrogen, others strong lines of calcium? The answer was not composition (all stars are 95 Hydrogen) but rather surface temperature.

As temperature increases, electrons are kicked up to higher levels (remember the Bohr model) by collisions with other atoms. Large atoms have more kinetic energy, and their electrons are excited first, followed by lower mass atoms.

If the collision is strong enough (high temperatures) then the electron is knocked off the atom and we say the atom is ionized. So as we go from low temperatures in stars (couple 1,000K) we see heavy atoms, like calcium and magnesium, in the stars spectrum. As the temperature increases, we see lighter atoms, such as Hydrogen (the heavier atoms are all ionized by this point and have no electrons to produce absorption lines).

### 1.1.3 H-R

Most of the things you can see in the night sky are stars: a few thousand are visible to the unaided eye. A star is a hot ball of mostly hydrogen gas; the Sun is an example of a typical, ordinary star. Gravity keeps the gas from evaporating into space, and pressure due to the star's high temperature and density keeps the ball from shrinking. In the core of the star, the temperature and densities are high enough to sustain nuclear fusion reactions, and the energy produced by these reactions works its way to the surface and radiates into space as heat and light. When the fuel for the fusion reactions is depleted, the structure of the star changes. The process of building up heavier elements from lighter ones by

4 CHAPTER 1. **LOCAL GROUP OF GALAXIES**

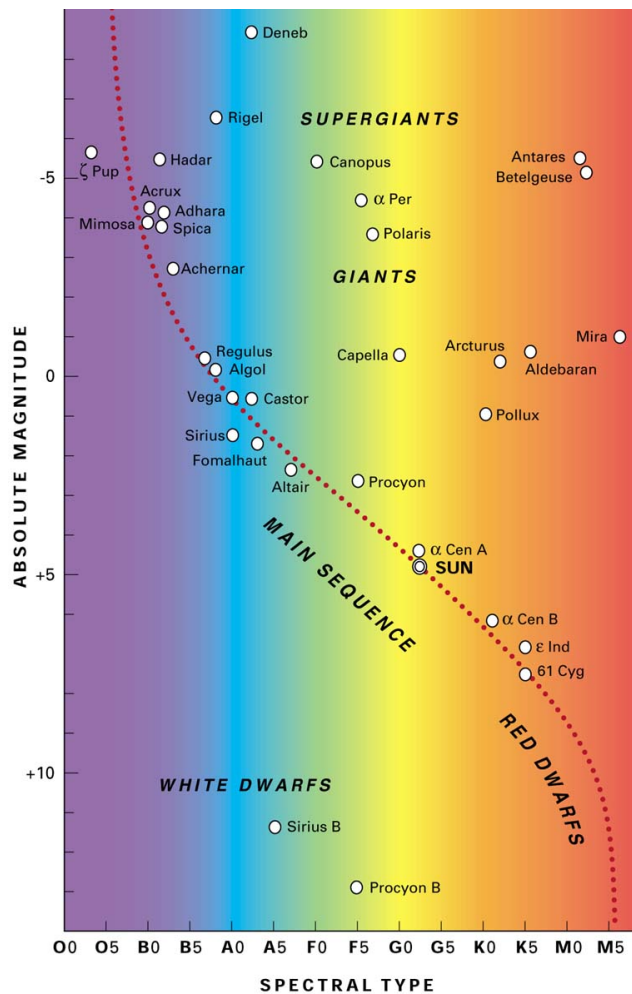


Figure 1.1.3: H-R diagram.

nuclear reactions, and adjusting the internal structure to balance gravity and pressure, is called stellar evolution.

Looking at a star through a telescope can tell us many of its important properties. The color of a star tells us its temperature, and the temperature depends on some combination of the star's mass and evolutionary phase. Usually, observations also allow us to find the luminosity of the star, or the rate at which it radiates energy as heat and light.

All stars visible to the unaided eye are in our galaxy, the Milky Way. The Milky Way is system of roughly 100 billion stars, along with a great deal of interstellar material. The galaxy is shaped like a flattened disk embedded in a round, faint halo. Gravity keeps the stars from drifting away, and the motions of the stars keep the system from falling in on itself. The Milky Way has no distinct edge - the distribution of stars tapers off gradually with increasing distance from the center. The SDSS detects stars more than a million times fainter than can be seen with the unaided eye, far enough to see the outer structure of the Milky

Way.

### Star Colors and Luminosities: The H-R Diagram

Astronomers often make plots of the luminosities of stars compared to their colors. The first such charts were made in the early twentieth century, when astronomers took spectra of thousands of stars, then placed the spectra into a sequence based on the appearance of several different features. The classes of stars were given different letters as names; in order of decreasing temperature, they are OBAFGKMLT. The hottest stars are class O, while the coolest are class T. Two astronomers, Ejnar Hertzsprung and Henry Norris Russell, independently started to wonder what would happen if they compared stars' luminosities to their spectral classifications (or, alternatively, to their temperatures). They knew that some stars were hotter and more luminous than the sun, and that others were cooler and less luminous. Hertzsprung and Russell found that 90 of the stars fell into a narrow band they termed the "main sequence." Today, we call this type of plot a Hertzsprung-Russell (or H-R) diagram.

Astronomers further divide each letter into ten categories from 0 to 9, with 0 being the hottest star in that spectral class and 9 being the coolest. So, a B1 star is hotter than a B2 star, and a B9 star is hotter than an A0 star. Our own sun is at the "hot" end of the G range with a surface temperature of 5,770 K; therefore, it's called a G2 star.

Spectral classes give us a convenient way to refer to most types of stars - from O0, the hottest at over  $25,000^{\circ}K$ , down to T9, the coolest failed stars at  $1,000^{\circ}K$ . Each spectral type of star is associated with a specific color: all G-type stars like the sun are yellow, all M-type stars appear red, and all B-type stars are bluish. Thus, this system of letters and numbers tells us where a star is on the horizontal (color or temperature) axis of the H-R diagram.

Two alternative systems tell us approximately where on the vertical (luminosity) axis a star can be found. One system uses absolute magnitude, a measure of luminosity derived from the apparent magnitude, or brightness of the star seen from Earth. The other system uses roman numerals, with the lowest numeral (I) for the most luminous stars (supergiants) and the highest numeral (V) for the less luminous (main sequence).

The tables below give the full classifications of spectral class and luminosity. The image below shows an H-R diagram for about a hundred typical stars. The bottom axis shows spectral class; the top axis shows temperature in degrees Kelvin. The left axis shows luminosity compared to the luminosity of the Sun (a "10" means the star is ten times more luminous than the Sun); the right axis shows absolute magnitude.

### Stellar Evolution

Stars are not static objects. As a star consumes fuel in its nuclear reactions, its structure and composition changes, affecting its color and luminosity. Thus, the H-R diagram not only shows us the colors and luminosities of many stars, it shows these stars at different stages in their evolutionary histories.

All stars on the main sequence have interiors hot enough fuse four hydrogen atoms into one Helium atom, and this one Helium atom is 0.7 lighter than 4 hydrogen atoms were. The lost mass is converted into energy, and this energy

## 6CHAPTER 1. **LOCAL GROUP OF GALAXIES**

Table 1.1.1: A schematic plot of the H-R diagram.

Spectral Classes	Temp ( $K$ )	Luminosity Classes	Class Star Type
O	> 25,000	I	Supergiant
B	11,000-25,000	II	Bright Giant
A	7,500-11,000	III	Giant
F	6,000-7,500	IV	Subgiant
G	5,000-6,000	V	Main Sequence, Dwarf
K	3,500-5,000	VI	Subwarf
M	2,200-3,500	VII	White Dwarf
L	1,600-2,200		
T	< 1,600		

is released, providing the star's luminosity. Over billions of years, however, the residual Helium in the star's core accumulates. When enough Helium has accumulated, the Helium can also undergo nuclear reaction. In this reaction, three Helium atoms are converted into one carbon atom. The Helium-burning nuclear reaction can occur only when the star's interior reaches a higher temperature, and this higher temperature causes the star's outer surface to expand to a much larger size than it was while it remained on the main sequence. Even though the core of the star is much hotter, the surface is now cooler, making the star redder. Thus, over time, a star becomes a red giant, moving from the main sequence area in the center of the H-R diagram to the red giant area in the upper right.

The evolution from main sequence to red giant occurs at different times for different stars. Stars that are much heavier and hotter, like O-stars, become red giants in only 10 million years. Cooler, lighter stars like our sun take 10 billion years to become red giants. This fact actually provides a way of testing how old a group of stars is - jut make an H-R diagram for the stars, and see which classes of stars have evolved off the main sequence!

Eventually, all the Helium in the core of the star is used up. At this point, what happens next depends on the mass of the star. The heaviest stars, over six to eight times as massive as our sun, have enough pressure in their cores to start fusing carbon. Once carbon is gone, they explode as supernovae, leaving behind neutron stars or a black holes. Less massive stars simply burn out, shedding their outer layers into beautiful planetary nebulae, and leaving the core as a hot white dwarf. White dwarfs lie in the lower left corner of the H-R diagram, a cosmic burial ground for dead stars.

### **Nebulae**

Originally, the word "nebulae" referred to almost any extended astronomical object (other than planets and comets). The word "nebulae" comes from the Greek word for "cloud". Before astronomers knew that galaxies were distant collections of stars, galaxies were also called nebulae because of their fuzzy appearance. Today, we reserve the word nebula for extended objects consisting

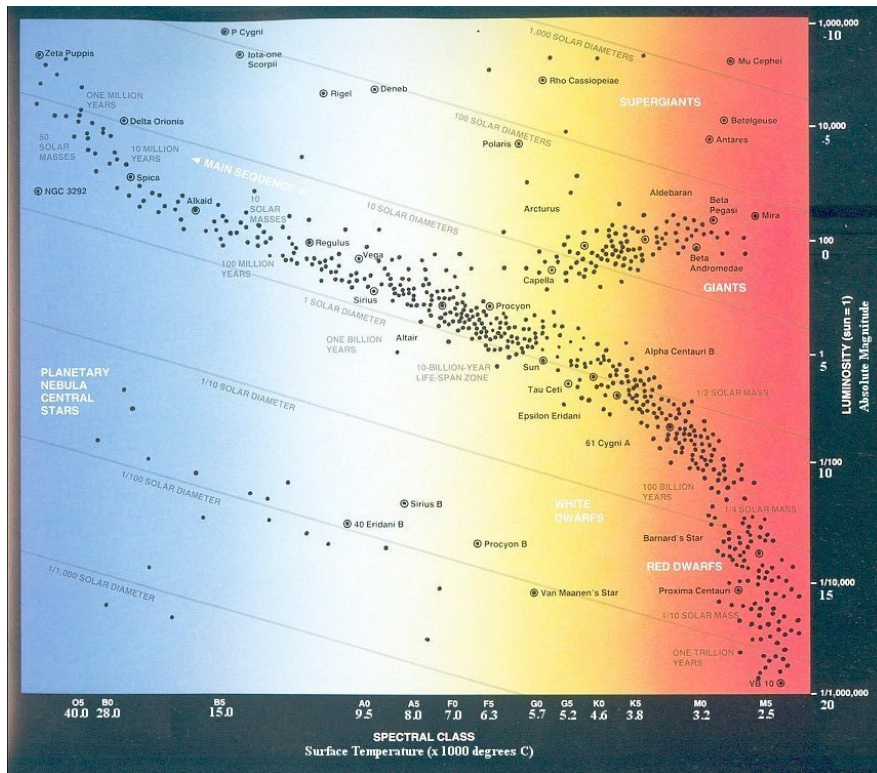


Figure 1.1.4: H-R Diagram

mostly of gas and dust.

Nebulae come in many shapes and sizes, and form in many ways. In some nebulae, stars form out of large clouds of gas and dust; once some stars have formed inside the cloud, their light illuminates the cloud, making it visible to us. These star formation regions are sites of emission and reflection nebulae, like the famous Orion Nebula.

Emission nebulae are clouds of high temperature gas. The atoms in the cloud are energized by ultraviolet light from a nearby star and emit radiation as they fall back into lower energy states (neon lights glow in much the same way). Emission nebulae are usually red, because Hydrogen, the most common gas in the universe, most commonly emits red light. Reflection nebulae are clouds of dust that simply reflect the light of a nearby star or stars. Reflection nebulae are usually blue, because blue light scatters more easily. Emission and reflection nebulae are often seen together and are sometimes both referred to as diffuse nebulae. In some nebulae, the star formation regions are so dense and thick that light cannot get through. Not surprisingly, these are called dark nebulae.

Another type of nebula, called a planetary nebula, results from the death of a star. When a star has burned through so much material that it can no longer sustain its own fusion reactions, the star's gravity causes it to collapse. As the star collapses, its interior heats up. The heating of the interior produces a stellar wind that lasts for a few thousand years and blows away the outer layers of the star. When the outer layers have blown away, the remaining core remnant

## 8CHAPTER 1. *LOCAL GROUP OF GALAXIES*

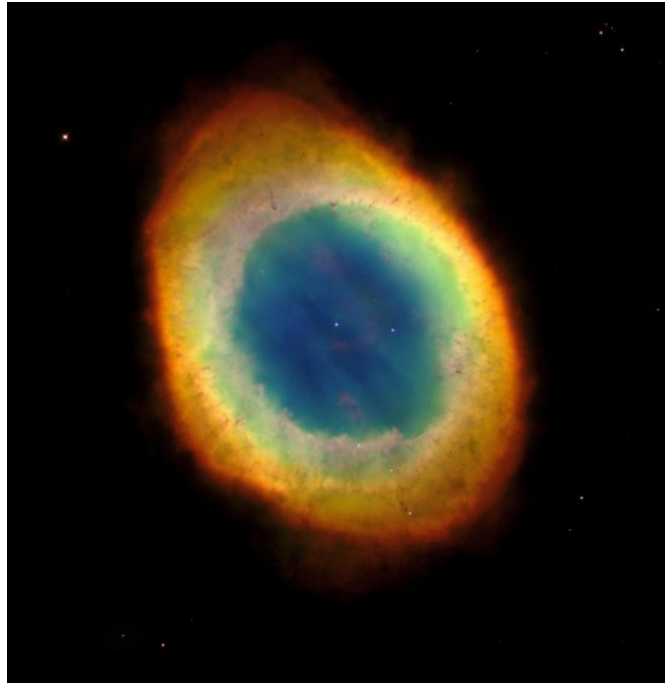


Figure 1.1.5: M 57 Planetary Nebulae.

heats the gases, which are now far from the star, and causes them to glow. The resulting "planetary nebulae" (so named because they look like gas giant planets through a telescope) are shells of glowing gas that surround a small core. Astronomers estimate that our galaxy contains about 10,000 planetary nebulae. Planetary nebulae are a common part of the normal stellar life cycle, but they are short-lived, lasting only about 25,000 years.

The life of a star whose mass is greater than 1.4 times the mass of the Sun ends more violently, and leaves behind a different type of nebula called a supernova remnant. When such a star runs out of fuel and collapses, an enormous shock wave sweeps through the star at high speed, blasting away various layers and leaving behind a core called a neutron star and an expanding shell of matter known as a supernova remnant. A supernova's shock wave is much more violent than the stellar wind that marks the end of a low mass star. Near the core of the remnant, electrons emit radiation called "synchrotron radiation" as they spiral toward the neutron star at speeds close to the speed of light. The ultraviolet portion of this radiation can strip electrons off, or "ionize" the outer filaments of the nebula, causing them to glow. In addition, the ejected matter sweeps up surrounding gas and dust as it expands, producing a shock wave that excites and ionizes the gas in the supernova remnant nebula, which is at low density but extremely hot (up to  $1,000,000^{\circ}K$ !). The most famous supernova remnant is the Crab Nebula in Taurus (M1). The light of the inner core is from synchrotron radiation, while the outer regions glow in many colors from emission of many gases, including red for hydrogen.

### 1.1.4 HII regions

A volume of ionized gas surrounding one or more young massive stars  $M < 20M_{\odot}$  with surface temperature ( $3 \times 10^4 K < T_* < 5 \times 10^4 K$ ) is termed an HII region. These stars, of spectral types O and B, are formed in giant molecular clouds and are generally grouped in "OB associations". They are strong sources of UV radiation, and emit significant fluxes of photons with energies higher than 13.6 eV (the ionization potential of hydrogen) giving rise to a region of ionized hydrogen around them, hence the name "HII region". The degree of ionization of the region is greater, the higher the temperature and the luminosity of the ionizing star(s) are.

It is well known that hydrogen is the major constituent of the interstellar gas and naturally also the major constituent of an HII region. However within these regions we also find other light elements in ionized states, notably He, O, N, C and Ne singly or multiply ionized.

The photoelectrons released in the ionization process (with local densities in the range  $10 - 14^4 cm^{-3}$  suffer collisions with other electrons and ions. In this way, they distribute their kinetic energy (given by the difference between the energy of the ionizing photon and the ionization potential of hydrogen) and maintain a Maxwellian velocity and distribution which defines the electron temperature of the HII region (typically in the range  $7000K < T_e < 1300K$ ).

Collisions between electrons and ions can excite some of the species in the region which then "forbidden" spectral lines (e.g. [OII], [OIII], [NII]). Among the most representative ions thus excited are  $O^+$ ,  $O^{++}$ ,  $N^+$ ,  $S^+$ ,  $S^{++}$ . These lines are termed forbidden because they result from a transition between a pair of levels, which violates the selection rules for electric dipole transitions. Their radiative downward transition probabilities are very low and the collisional de-excitation probability is even smaller if the density is very low. Also, recombination of these thermalized electrons with ions in excited states, followed by a cascade downwards in energy level gives rise to recombination lines, notably of  $H^+$  and  $He^+$ . These two types of line emission dominate the emission spectrum of an HII region.

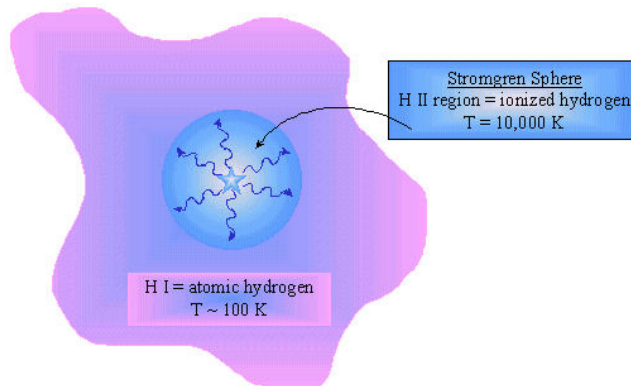


Figure 1.1.6: Stromgren sphere.

**1.1.5 Structure of an HII region**

Within an HII region Hydrogen, which makes up over 75% of the mass, is virtually fully ionized. We will take the ionization structure of the Hydrogen as a first approximation to the overall structure of the region. The radius of the region, the "*Strömgrenradius*" ( $R_s$ ), is the radius which defines the volume ( $\frac{4}{3}\pi R_s^3$ ) within the number of ionizing photons emitted by the ionizing star(s) per unit time ( $N_*$ ) just equals the number per unit time of recombinations of electrons with ions. The flux falls with increasing distance from the emitting star(s), due both to purely geometrical dilution and to absorption along the paths of the photons, until it reaches a level where the ionizations and the recombinations just balance, which is at the *Strömgrenradius*. In computing this we assume that the region as a whole is optically thick and that the "on the spot" assumption is valid, i.e. there is a high probability of absorption of ionizing photons and that recombinations to the ground state at any point in the region release photons which are absorbed immediately nearby, with no net effect on the overall ionization balance in the region. With these assumptions the *Strömgrenradius*,  $R_s$ , by

$$N_* = \int_{\nu_0}^{\infty} \frac{L_{\nu}}{h\nu} d\nu = \frac{4}{3}\pi R_s^3 N_H^2 \alpha_B \quad (1.1.1)$$

where  $\nu_0$  is the threshold frequency for ionizing the hydrogen (the "Lyman limit" frequency),  $L_{\nu}$  is the luminosity of the stars per unit frequency interval,  $N_H$  the hydrogen number density in atoms  $cm^{-3}$ , and  $\alpha_B$  is the recombination coefficient to excited levels of the hydrogen.

At radius  $R_s$  there is a (geometrically) well defined transition between an effectively fully ionized sphere of Hydrogen and the surrounding cloud of neutral H. For a mean interstellar density of 1 atom  $cm^{-3}$ , the theoretical *Strömgrensphere* has a radius of 108 pc for a single O5 star and 23 pc for a B0 star. The transition zone thickness between fully ionized neutral H is  $d \approx (N_H a_{\nu})^{-1}$  0.1 pc where ( $a_{\nu}$  is the ionization cross section for Hydrogen), which is the mean free path of an ionizing photon at the edge of the region and is negligible compared to  $R_s$ . For the other elements in the region, their degree of ionization depends on the distance from the central ionizing star and its effective temperature.

The second most abundant element after Hydrogen is Helium, whose first ionization potential 24.6 eV, and whose second ionization potential is 54.4 eV, so that there is very little doubly ionized He in HII regions, since even the hottest O stars hardly emit photons more energetic than 54.4 eV. In general, those photons with  $13.6eV < h\nu < 24.6eV$  ionize the Hydrogen, and those with  $h\nu > 24.6eV$  ionize the Helium. According to the element abundances and the spectrum of the ionizing star(s) we find different ionization structures within an HII region. A qualitative scheme is presented in Figure below.

As we can see from the figure, a star which emits few photons with  $h\nu > 24.26eV$  will be surrounded by a small cloud (within which these energetic photons are absorbed) of  $H^+$  and  $He^+$ , in which less abundant species such as  $O^{++}$ ,  $N^{++}$  and even  $Ne^{++}$  may be found, since the second ionization potentials of O, N and Ne are 34.0 eV, 29.5 eV and 41.1 eV respectively. This central cloud will be in turn surrounded by a much larger cloud of  $H^+$  and  $He^o$  together with heavier atoms in their lowest states:  $O^+$ ,  $N^+$ ,  $Ne^+$ .

However, a star which emits a large flux of photons with energies greater

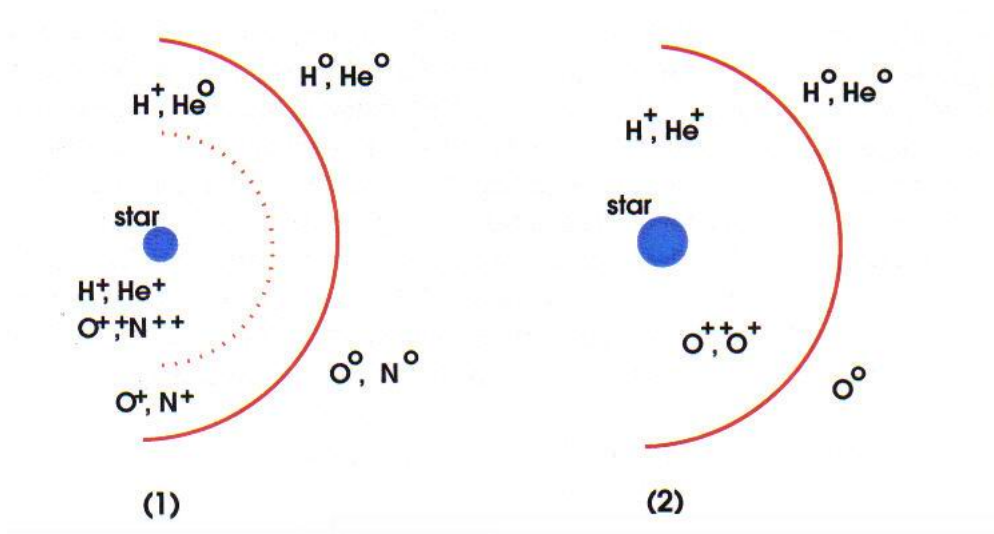


Figure 1.1.7: Stratification of the ions within HII regions for different temperatures of their ionizing stars:(1) $T_* \leq 4000K$ , (2) $T_* > 4000 K$

than 24.6 eV (i.e. a star with  $T_* > 40000K$ ) will ionize H and He together, i.e. will produce a volume where  $H^+$  and  $He^+$  coexist, but no a region where the Hydrogen is ionized and the Helium is neutral. In a similar manner to the first star, in this case too, photons not absorbed in ionizing H and He will ionize the heavier elements. There will be O, N and Ne in high ionization states in the centre of the HII region and in the singly ionized state near the transition from  $H^+$  to  $H^0$  at the edge of the region. Observations show that the structures are obviously more complex than described here, but that this description is a valid practical guide to the global phenomenology.

### 1.1.6 Populations of HII regions in irregular galaxies

Spiral and irregular galaxies contain relatively large numbers of HII regions, in contrast with ellipticals and lenticulars, which hardly have any. Since HII regions form around young hot stars they are excellent tracers of recent star formation, which makes spirals the best laboratories for star formation studies. Although the number of regions does vary from galaxy to galaxy, it is normal in most galaxies to find them concentrated along the spiral arms and serving to define them in the plane of the galaxy. The study of an HII region populations is of great relevance for understanding a number of aspects galaxies:

- **Abundances.** Although HII region emission spectra have many features in common, there are differences, notably in their heavier element (metal) content. These metals are present as a result of the nuclear burning processes within stars, which subsequently expel the metals into their interstellar environments via winds or explosions. Measurement of abundances in HII regions is a good way to estimate the net effects of stellar evolution on the environment for new star formation within galaxies.

- **Velocity fields.** As the light from HII regions is concentrated into a relatively small number of narrow spectral emissions lines, they are excellent tracers of radial velocity, which can be measured via the Doppler effect. This, together with the normally galaxy-wide distribution of the regions, allows us to use them to measure velocity fields within galaxies. Naturally we are limited by the need to recover by projection a three-dimensional field from the one-dimensional velocity information, and normally offer significantly higher spatial resolution than their alternatives: essentially the 21 cm line of HI and the rotational lines of CO. Frequently, 21 cm emission comes from a more unbroken area of a galaxy than the emission lines from HII regions, which are discrete, so that HII region emission lines and the 21 cm line offer complementary data for the interpretation of the kinematics of a galaxy. One of the best emission lines for these measurements is H, since it is intense, and emitted in a spectral region where CCD detectors have their maximum sensitivity. There are zones of galaxies where the gas flows in orbits which are non-circular, due to departures from axisymmetry in the underlying gravitational structure. Typical zones of this type are found around bars, where gas orbits tend to oval shapes with the bar major axis as their long axis, also in spiral arms, where the density wave system sets up gas streaming motions across the arm. Other types of global non-circular motions include motion perpendicular to the galactic plane due to outflow from regions of strong star formation, notably around the galactic nucleus and also in the disc, concentrated in the spiral arms. In addition there may be strong local motions, above all turbulence within regions of active star formation. Observations of HII regions, notably in H, yield information about all these phenomena and make the purely kinematic study of HII region emission lines from complete populations of key importance in extragalactic astronomy.
- **Luminosity function.** For an HII region to exist, the presence of one or more O or B stars (or possibly Wolf-Rayet stars), is necessary, in a zone with a relatively high gas density. As the lifetime of such stars is short:  $10^6$  to  $10^7$  years and in any case much shorter than the lifetime of a galaxy, it is clear that HII regions show us where recent massive star formation has taken place. It is thus clear, also, that the study of the distribution of these regions in an irregular galaxy, and of their luminosity function, will yield valuable clues about the parameters which govern massive star formation. There have been a number of studies in this field: Kennicutt (1984), Hodge (1987), Edgar & Hodge (1989), Rand (1992) are the authors whose earlier work forms much of the basis of present-day research. Among the more recent work on the luminosity functions of the regions and their physical properties, we can cite Rozas et al. (1996a,b) and subsequent papers from our own group. The study of the statistical properties of complete populations of HII regions by the H emission line is, therefore, not only of interest for what it tells us about the properties of the regions themselves and about a global kinematics of a galaxy, but also because we can learn much about the properties of massive star forming regions and the effects on these of a number of possibly relevant parameters: dynamics, metallicity, galaxy size, etc.

The importance of this type work has been clear since the studies of Kenni-

cutt et al. (1989), for spiral and irregular galaxies. In this and subsequent work, e.g. Rozas et al. (1996a), Rand (1992), Cepa et al. (1989, 1990), Knapen et al. (1993), Gonzalez-Deglado & Perez (1997), Tsvetanov & Petrosian (1995), it was found that the luminosity function (LF) of HII regions in H can be fitted with a power law of type:

$$dN = AL^n dL \quad (1.1.2)$$

where  $dN$  is the number of regions in the luminosity range type between  $L$  and  $L+dL$ , and where  $n$  is a constant which takes a value of  $n = 2 \pm 0.5$ , in which the variation is not an uncertainty, but rather represents a true variation between one galaxy and another.



# Chapter 2

## Studies in the galaxies IC 10 and Sextan B

### 2.1 Introduction

Most of the galaxies in the Local Group (LG) are dwarf irregulars and spheroidals. These morphological types also represent the most numerous objects in the nearby universe, but can be studied in great detail only at the close distance of the Local Group. We are performing a narrow- and broad-band filter survey, the Local Group Census, which is mainly aimed at studying all classes of emission-line populations in the Local Group.

#### 2.1.1 IC 10

IC 10 is an irregular galaxy in the constellation Cassiopeia. It was discovered by Lewis Swift in 1889. Nicholas U. Mayall was the first to suggest that the object is extragalactic in 1935. Edwin Hubble suspected it might belong to the Local Group of galaxies, but its status remained uncertain for decades. Radial velocity of the galaxy was measured in 1962, which strengthened the assumption. Finally, in 1996, based on direct Cepheid distance measurements, it was demonstrated to be a true member of the group. Despite its closeness, the galaxy is rather difficult to study because it lies near the plane of the Milky Way and is therefore heavily obscured by interstellar matter.

Apparent distance between IC 10 and the Andromeda Galaxy is about the same as the apparent distance between the Andromeda Galaxy and the Triangulum Galaxy, which suggests that IC 10 may belong to the M31 subgroup.

IC 10 is the only known starburst galaxy in the Local Group of galaxies. It has many more Wolf-Rayet stars per square kiloparsec ( $5.1 \text{ stars/kpc}^2$ ) compared to the Large Magellanic Cloud ( $2.0 \text{ stars/kpc}$ ) and Small Magellanic Cloud ( $0.9 \text{ stars/kpc}^2$ ). Although the galaxy has similar luminosity to the SMC, it is considerably smaller. The higher oxygen level in the galaxy compared to the SMC suggests that the star formation activity has continued for a longer time period. The evolutionary status of the Wolf-Rayet stars suggests that they all formed in a relatively short timespan. Ratio between two types of Wolf-Rayet stars in IC 10 is very different from the ratio in other galaxies in the Local Group, which may be somehow due to the starburst nature of the galaxy. Currently the



Figure 2.1.1: IC 10 galaxy.

galaxy produces stars at the speed of 0.04-0.08 MSun per year, which means that the gas supply in the galaxy can last only a few thousand million years.

Table 2.1.1: Parameters of IC 10 galaxy.

Type	Ir V
Right ascension	0.0h 20m 24s
Declination	+59°17'30"
Distance	$2.2 \pm 0.2$ millionly
Apparent magnitude	$+10.4 \pm 0.2$
Apparent dimensions	$5.5' \times 7.0'$
Constellation	Cassiopeia
Radius	$18,000 \times 21,000$ ly

The galaxy has a huge envelope of Hydrogen gas, apparent size measuring  $68' \times 80'$ , which is by far larger than the apparent size of the galaxy in visible light ( $5.5' \times 7.0'$ ). IC 10 is also unusual in the respect that the visible part of the galaxy seems to rotate different direction than the outer envelope.

IC 10 is a highly obscured galaxy ( $E(B - V) \cong 0.85$ ), located at a low Galactic latitude  $b = -3.3$ . Its distance and its position (only 18 apart from M31 on the sky) suggest a possible membership to the M31 subgroup (vdB00). It is the only starburst galaxy in the Local Group, and the presence of a large number of HII regions proves that it is undergoing massive star formation. IC

10 is a rather small galaxy with an effective radius  $r = 0.5$  kpc, only one half the effective radius of the Small Magellanic Cloud (SMG), whereas their luminosities are comparable. Its oxygen abundance is higher than that of SMC, showing a higher past rate of star formation. This galaxy is clearly resolved in stars on ground-based images, and a large number of Wolf-Rayet stars is known. The presence of a large foreground extinction due to its location in a direction close to the Galactic plane has prevented so far deep studies of the stellar populations.

### 2.1.2 Sextan B

Sextans B is a dIrr at a distance of 1.36 Mpc (Karachentsev et al. 2002). Like in Sextans A, the star formation history has likely been complex, with long periods of relatively low star formation rates punctuated by periods of short star-forming bursts (Tosi et al. 1991; Sakai et al. 1997). As far as its global properties are concerned, Sextans B is considered to be a "twin" of Sextans A, but Sextans B is of particular interest because the previous measurements of the nebular oxygen abundance for this galaxy by Stasinska et al. (1986), SKH89, and Moles et al. (1990, hereafter MAM90) differ considerably. Sextans A and Sextans B are both dwarf irregular galaxies (Ir V and Ir IV-V morphological types, respectively, cf. van den Bergh 2000, hereafter vdB00) with approximately the same V luminosity and located at a very similar distance (1.3 Mpc, Dolphin et al. 2003 for Sextans A and vdB00 for Sextans B). Their separation in the sky is also relatively small (10 degrees), which corresponds to about 280 kpc at the adopted distance. Moreover their velocity difference is only  $23 \pm 6 \text{ km s}^{-1}$ . All these properties suggest a common formation for these two galaxies, probably together with NGC 3109 and the Antlia galaxy, also at a similar distance and location in the sky. Considering the mean distance of the four galaxies from the barycentre of the Local Group (LG), 1.7 Mpc, this sub-group is located beyond the zero velocity surface of the LG (cf. vdB00) and can be considered the nearest external group of galaxies. Then these galaxies are particularly interesting as they represent a group of dwarf galaxies relatively isolated from giant galaxies.

In dIrr galaxies, star formation is generally active, as shown by the conspicuous number of HII regions that they contain. There are several photometric and spectroscopic studies of HII regions in both galaxies. Photometry of HII regions in Sextans A was obtained by Hodge (1974), Aparicio & Rodriguez-Ulloa (1992), and Hodge et al. (1994), the latter one being the most complete survey with 25 HII regions detected. Hunter et al. (1993) studied large ionized gas structures outside normal HII regions, like shells and filaments generated by the action of massive stars through winds and supernova explosions. Spectra of four HII regions were obtained by Skillman et al. (1989), from which an oxygen abundance was derived. The brightest HII regions of Sextans B were first catalogued by Hodge (1974). Strobel et al. (1991) classified twelve HII regions, whereas oxygen abundance was derived for four HII regions by Skillman et al. (1989). Note, however, that these spectroscopic studies were generally not deep enough (except for one or two objects) to allow direct measurement of the nebular electron temperature via detection of the [OIII] 436.3 nm line, causing an important source of uncertainty in the determination of their chemical abundances.



Figure 2.1.2: Sextan B galaxy.

Table 2.1.2: Parameters of Sextan B galaxy.

Type	Ir V
Right ascension	10h 00m 00s
Declination	+05°20'00"
Distance	4.7 million ly
Apparent magnitude	+11
Apparent dimensions	5.1' × 3.5'
Constellation	Sextans

# Chapter 3

## Observations and Data reduction

### 3.1 Observations

The observations were made with 2.5m Isaac Newton Telescope (INT) and the prime focus Wide Field Camera (WFC). So, let' s give a report about the technical characteristics of the telescope and the camera.

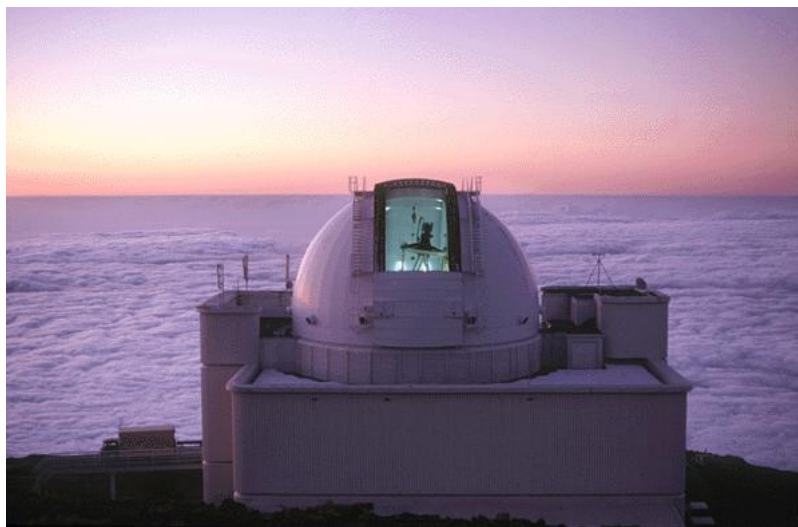


Figure 3.1.1: Dome of Isaac Newton Telescope.

The born-again INT, at La Palma, differs significantly in its mechanics, electronics and optics from the earlier incarnation at Herstmonceux. The change in latitude from 50 degrees 51 minutes 58 seconds to 28 degrees 45 minutes 43.4 seconds has resulted in a large change of angle to the polar disc which stands almost on edge. A segment was removed from the disc in order to allow operation to a declination of -30 degrees. New encoders and drive electronics were fitted and a new computer control system was written. The primary mirror was replaced with a slightly larger one (from 98 inches to 100 inches) of considerably higher optical quality made of low-expansion material. The old prime-focus assembly, which required a caged observer, was replaced with one operated

entirely by remote control; similarly, the Acquisition and Guidance Box at the Cassegrain focus is completely new. The telescope is housed in a new dome, the old one being left as a landmark for channel shipping. Finally, there is a suite of new instruments and a computer system to control them.

The mechanical structure of the INT was shipped to La Palma in 1981 and was re-erected into the bare frame of its building in 1982. The mirror arrived on the island on December 10, 1982; the building was handed over by the contractors to the RGO on January 17, 1983 and work began on preparing the laboratories and workshops for the commissioning of the telescope. The first of three direct air shipments of machinery, instruments and computers arrived on La Palma on January 25. By September the building was in full operation and the telescope was fully assembled, with a freshly aluminised mirror, by the end of the year. On the first night of February 1984 stars were first seen in the telescope, at the prime focus. The telescope commissioning programme had been targeted towards the completion of the Cassegrain spectrograph since this would be the most widely demanded instrument; it was also tolerant to telescope pointing and tracking.

In the spring of 1984 there was a concentrated effort to commission the Cassegrain instrumentation, including acquisition TV cameras, Intermediate Dispersion Spectrograph (IDS), IPCS and CCD detectors and ADAM, the software environment which brings together this complex of instruments into one working station. This programme was completed in May.

On May 29 1984, the telescope welcomed its first scheduled astronomer. It operated for astronomers for 47% of the time in the first six-month period (Semester F), 50% in semester G, 62% in Semester H and 73% in Semester I. The rest of the time was used for engineering work.

The optical telescope assembly weighs 51,361 kg and including the mounting 85,361 kg.

### **The Mounting**

The telescope has a polar disc/fork type equatorial mounting supported by five axial and three radial hydrostatic oil bearing pads. The tube, a conventional open Serrurier truss structure, supports the prime-focus assembly or secondary mirror for Cassegrain and Coude operation.

Declination coverage was improved when moved to La Palma by cutting a sector out of the polar disc, and by a redesign of the dome aperture (a proposal to remount the telescope on an altazimuth mount was found to have some attractive features, but was rejected because of extra costs.) Drive limits are currently set at -30 degrees Declination, 70 degrees zenith distance and 6h Hour Angle (operation below the pole is also possible).

DC servo motors with integral tachogenerators are used for the slow-motion drives on both arms. The RA axis is driven by a worm/worm-wheel assembly and the Declination axis by a recirculating ball screw and nut. Preload and quick motion drive are provided by a pair of motors driving through spur gearing.

The telescope's position is determined by Moire fringe grating encoders mounted on each axis. There are three reading heads per axis. One bit corresponds to 0.3 arc sec in RA and 1 arc sec in Declination, although systematic errors are larger. When the telescope is being driven by the slow-motion motors,

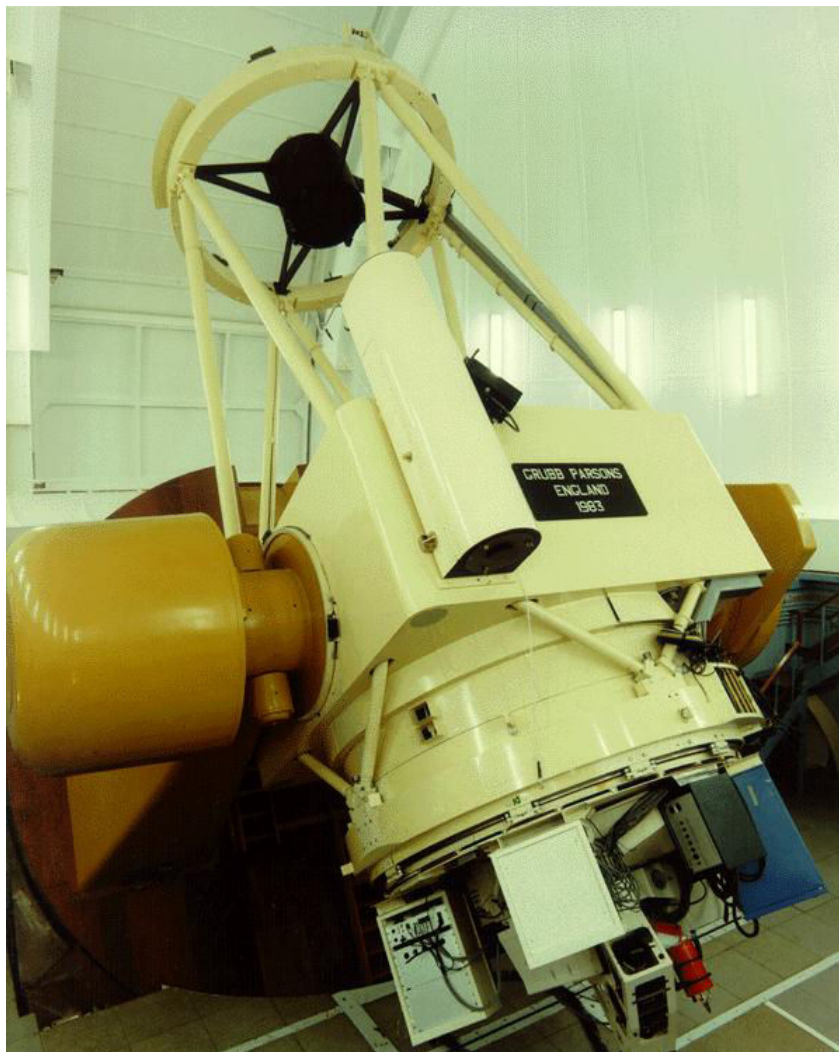


Figure 3.1.2: Isaac Newton Telescope.

optical incremental encoders are used, with resolutions of 0.01875 and 0.01 arc sec in RA and Declination, respectively, mounted on the drive shafts.

The pointing model for the INT comprises the standard errors of an equatorially mounted telescope (offsets in Hour Angle and Declination, collimation error, misalignment of the polar axis and non-perpendicularity of axes), together with an empirical (Fourier series and polynomial) model of flexure in the telescope structure and large-scale errors in the encoder readings. The r.m.s. errors in the absolute pointing of the INT are always less than 5 arc sec; values between 2.8 and 4.5 arc sec were obtained during tests at Prime and Cassegrain foci during 1985. Short-term tracking errors are less than 0.25 arc sec; longer-term drifts are removed by the autoguiders.

**Telescope limits:**Zenith distance  $< 70$  $-6h < \text{hour angle} < +6h$ (above pole)Declination  $> -30^{\circ}09'30''$ 

Operation below the pole is possible, but only gains a small extra area of sky; consider it in exceptional circumstances.

The lower windshield causes vignetting for zenith distances  $> 57^{\circ}$  and is raised for such observations.

**The Optics**

The optical system of the INT is a conventional Cassegrain with a paraboloidal primary mirror and a hyperboloidal secondary. The primary has a diameter of 2.54-m (the original 98-inch primary mirror was replaced by a 100-inch mirror when the INT was moved to La Palma) and a focal length of 7.475-m, giving a focal ratio of  $f/2.94$  at the uncorrected primary focus. It weighs 4,361 kg and it is made of Zerodur and has a negligible coefficient of expansion ( $10^{-7}K^{-1}$  approximately). On axis, 80% of the light from a point image lies within a circle of 0.3 arc sec in diameter. A three-element corrector with a flat rear surface and increased back focal distance, is used at the prime focus to give an unvignetted field of 40 arc min at a scale of 24.68 arc sec/mm. The images are calculated to be smaller than 0.5 arc sec diameter everywhere over the unvignetted field for incident wavelengths in the range 3650Å to 10140Å. The two secondary mirrors give  $f/8$  Cassegrain and  $f/50$  Coude foci (although the latter was never implemented). The scale at the Cassegrain focus is 5.41 arc sec/mm and the unvignetted field is 20 arc min.

Table 3.1.1: Optical characteristics of INT.

	Prime Focus	Cassegrain Focus
Focal Length (mm)	8357	38130
Focal ratio	$f/3.29$	$f/15$
<b>Field Diameter (arcmin)</b>		
- no vignetting	40	20
- 50 % vignetting	52	22
Scale (arcsec/mm)	24.7	5.41
Diameter of Central Obstruction (mm)	914	914

The WFC designed and built by: Royal Greenwich Observatory (United Kingdom), Kapteyn Sterrenwacht Werkgroep (Holland) and the Lawrence Berkeley Laboratories (California). The pixel size of WFC is 0.33 arc / pixel, the gain is 2.8 electrons / ADU and the readout noise 6.2 electrons. A lot of data were taken from 2001 and 2002. Most of the nights were photometric. The average seeing was 1.42" and the exposure time was about 1200 seconds with narrow band filters and 400 seconds for the broad band filters. We used the filters Ha, SII, stY, OIII, HeII, R, g,  $\lambda$  6568/95Å,  $\lambda$  6725/80Å,  $\lambda$  5505/240Å,  $\lambda$  5008/100Å,  $\lambda$  4686/100Å,  $\lambda$  6380/1520Å,  $\lambda$  4846/1285Å respectively. The Ha

filter includes the NII line and the OIII includes 52,9 % of OIII  $\lambda$  4959Å. At the Figures 3.1.4 and 3.2.1 you can see the ING's filters response and the WFC. For the photometric calibration we used standard spectrophotometric stars like BD28, Feige110, Hz44 and Sp1942. For the Flat and Bias correction we used the INT's pipeline "GIGAWULF" (GIGAWULF: Powering the Isaac Newton Group's Data Pipeline, Greimel. R, R. 2001, in ASP Conf. Ser., Vol. 238). More information about the observations you can find in the follow Table 3.1.1.

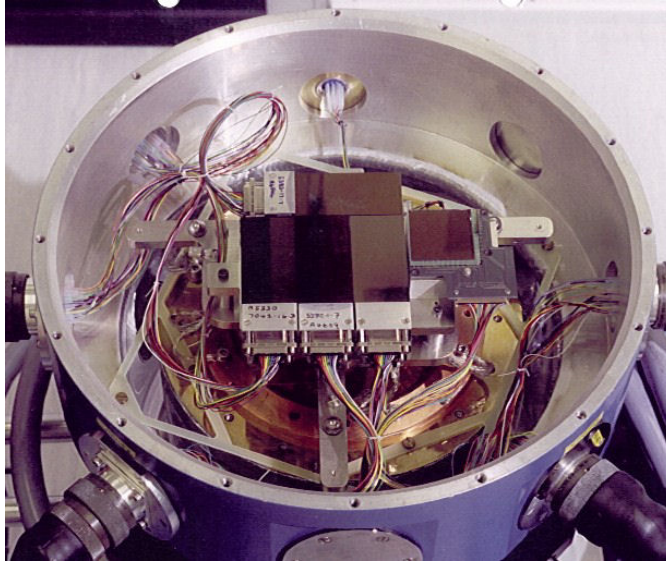


Figure 3.1.3: The Wide Field Camera.

Table 3.1.2: Information about the observations.

FIELD	ON BAND filter/exp. time	OFF BAND filter/exp. time	PHOTOM.	SEEING
<b>NE</b>				
Ha	Ha/3x1200s	R/3x300s	yes	0.71 <sup>''</sup>
OIII	OIII/3x1200s	stY/3x300s	yes	1.80 <sup>''</sup>
SII	SII/3x1200s	R, Ha/3x300s/1200s	yes	
He	He/3x1200s	stY/3x300s	yes	
<b>NW</b>				
Ha	Ha/3x1200s	R/3x300s	yes	1.31 <sup>''</sup>
OIII	OIII/3x1200s	stY/3x300s	yes	1.31 <sup>''</sup>
SII	SII/3x1200s	R, Ha/3x300s/1200s	yes	1.37 <sup>''</sup>
He	He/3x1200s	stY/3x300s	yes	1.63 <sup>''</sup>
<b>SW</b>				
Ha	Ha/3x1200	R/3x1200	yes	1.19 <sup>''</sup>
SII	SII/3x1200	R,Ha/3x300/1200	yes	2.02 <sup>''</sup>

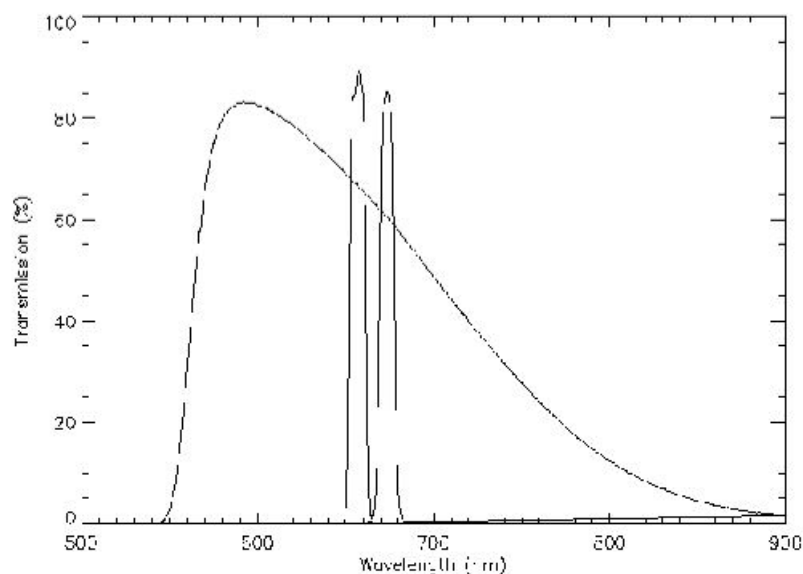


Figure 3.1.4: The filters R (Harris), H, SII.

## 3.2 Data Reduction

### 3.2.1 Image distortion

For the reduction we used the **IRAF** package, but let's talk a little about the telescope field. The WFC has a large field of view. It use 4 CCDs (4K x 2K) and it covers 33 arcmins at the sky. For this reason at the edges of the frames we have very big distortion. Every filter has different distortion factor and this makes the work more complicate. So, it's nessecery to correct this distortion but before that, we need to make an align correction because the data from the INT have not perfect alignment. We must align all frames. To do this we used the *imalign* command. First we create a list.coo file with the coordinate of some good stars (not saturated) from the reference image (for example image1.fit). Then we estimate the shift between the frames and we create an other file (shift.txt) with these shifts. After that we can run the *imalign*. We type the following:

```
cl> epar imalign
input:          image1,image2,image3 .....,
referen. image: image1
coords file:    list.coo
out put       :  test1,test2,test3 .....,
shift         :  shift.txt
boxsize       :  must be bigger than the biggest error value
```

The input images could be all the images per filter and after the

`imcombine`

command we can align again the output images. When

`imalign`

finishes we have the new aligned images `test1`, `test2`, `test3` ... Now we are ready to combine the frames from every filter.

```
cl> imcombine test1, test2, test3 test
```

where ‘test’ is the output frame.

We combine the images in the same filters. So, after we combine all fields, we have only one image per filter. If this images are alinged, **IRAF** can estimate the distortion in one filter (in our case H) and can apply that distortion into the other frames. In optics, image distortion is a divergence from rectilinear projection caused by a change in magnification with increasing distance from the optical axis of an optical system. Then, we can subtract the images properly. In `ap`hot/`digiphot`/`noao` we type:

```
ap>centerpars.cbox=30
ap>phot image =image1 coords=list.coo
ap>txd textfile=image1.mag.1 fields=xin,yin,xcenter,ycenter expr=yes>image1.file
ap>del image1.mag.1
ap>geomap image1.file image1.tran 1 2047 1 4098
ap>geotran image1 outputfile image1.tran image1.file
ap>del image1.file
ap>del image1.tran
```

‘Phot’ does the photometry, ‘geomap’ creates a distortion map and ‘geotran’ applies the distortion to the image.

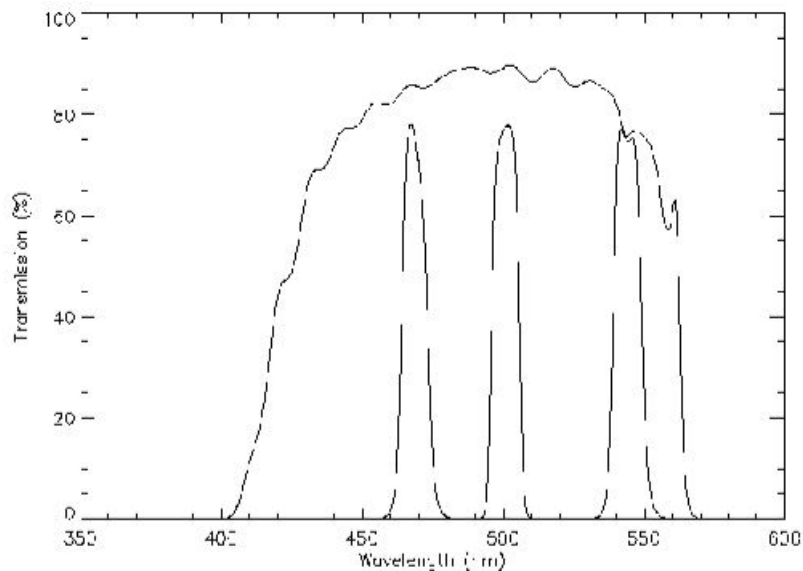


Figure 3.2.1: The transmission curves of filters `g`, `He`, `OIII` and `stY`.

We did the same with all the images.

**3.2.2 Continuum subtraction**

This is the most difficult part of the reduction. The aim is to subtract the continuum of the spectra continuum emission from the observations taken through the narrow band filters, in order to leave only the flux emitted by the spectra emission lines of our interest. We used the filters R (Harris) for the Ha and SII, stY for the OIII and g for the He. As we said before, we used different exposure time for each filter and this means that we need to estimate the scale factor between them. So, we normalized the frames to *ADUs/sec*, and then we estimate the scale factor of the continuum (R, stY, g) images, so that when subtracted from the narrow band images, would give us images free of continuum emission. But, as we can see in the Figures 3.1.4 and 3.2.1, the broad band filters include already some important emission lines. If we just subtract the broad band images from the narrow band ones, we are going to oversubtract the continuum, losing some relevant emission line. For this reason we used some equations from Roberto Terlevich to correct this quantity (“High-resolution surface photometry of the core of NGC 4151” Roberto Terlevich, Mon. Not.R astr. Soc. (1991) 249, 36-45). These are:

$$Ha = \frac{Ha-f1*R}{t_{Ha}-t_R*f1} \quad (1) \quad (H : \text{emission from non continuum subtracted image})$$

$$SII = \frac{SII-R*f2+t_R*f2*Ha}{t_{SII}-f2*t_R} \quad (2) \quad (H: \text{emission from continuum subtracted image})$$

f1: scale factor Ha-R

f2: scale factor SII-R

$t_{Ha}$  : Ha filter transmission

$t_R$  : R filter transmission

$t_{SII}$ : SII filter transmission

The transmission values for the INT’s filters Ha, R and SII are:

$$t_{Ha} = 0.89$$

$$t_R = 0.88$$

$$t_{SII} = 0.84$$

Also, because the different filters, are different, the frames that we took through the stY, He and OIII filters have different FWHM than the rest. This means that we can not subtract them properly. To solve this problem we used the

`'gauss'`

command to smooth them until the correct FWHM. When everything is ready. We subtract the frames using the command

`'imarith'`

.

```
cl>gauss test1 output 1.2
```

```
cl>imarith test1 - test2 test
```

where “test” is the output image

### 3.2.3 Flux calibration

For the flux calibration we used some spectral-photometric stars. Of course it is necessary to have standards stars in all narrow band filters. Before proceeding any further we need to use the measurements from the fluxes of these stars. This will be later compared to the calibrated flux (in  $erg/sec/cm^2$ ) emitted by the standard stars. First we combined the images from the same filters and then we did the photometry. **Apphot** is a very good package for the point sources photometry. We used the measurements from 2 standard stars. Feige 110 and the BD +28 4211. These data were taken by Corradi, Zurita, Mislis, from NGC6822 Photometric Atlas in HII regions. They compared three packages for that. Daophot, **Apphot** and Gaia. The results are shown in Table 3.2.1

Table 3.2.1: Standard Stars Photometry

BD +28 4211	Flux (ADUs/sec)	Mag	% Error from real value
Real Value		10.89	
Daophot	19450.3	9.832	9.72 %
Apphot	7070.19	10.93	4.00 %
Gaia	19260.3		9.63 %
Feige 110			
Real Value		12.10	
Daophot	5425.04	10.78	10.9 %
Apphot	2521.29	11.86	1.98 %
Gaia	8081.75		17.1 %

As we can see the **Apphot** package gives the smallest % error for the point source photometry. The fluxes from Apphot were in ADUs, and if we divide by the exposure time, we have ADUs/sec. To transform the fluxes from ADUs to  $erg/sec/cm^2$  it's not so hard. First of all we know the transmission curve for all the filters (Figures 3.1.4 and 3.2.1). On the other hand we have all information that we need from the standard star, the flux calibrated spectra. In every value of wavelength there is a value of the magnitude. So in every filter we expect a different magnitude value, as we can see in Figure 3.2.2 below.

We are ready now to use the equation 3.2.1 below

$$FLUX = \int_{\Delta\lambda} \left( \frac{3 * 10^{18}}{\lambda^2} * 10^{\frac{mag+48.60}{-2.5}} \right) d\lambda \text{ in } erg/sec/cm^2 \quad (3.2.1)$$

and then using the equation 3.2.2 we can estimate the calibration factor for this night's data.

$$CalibrationFactor(CF) = \frac{ADU(newdata)}{IntergractionTime} * \frac{FLUX(erg/sec/cm^2)}{ADU(Calibrationstar)} \quad (3.2.2)$$

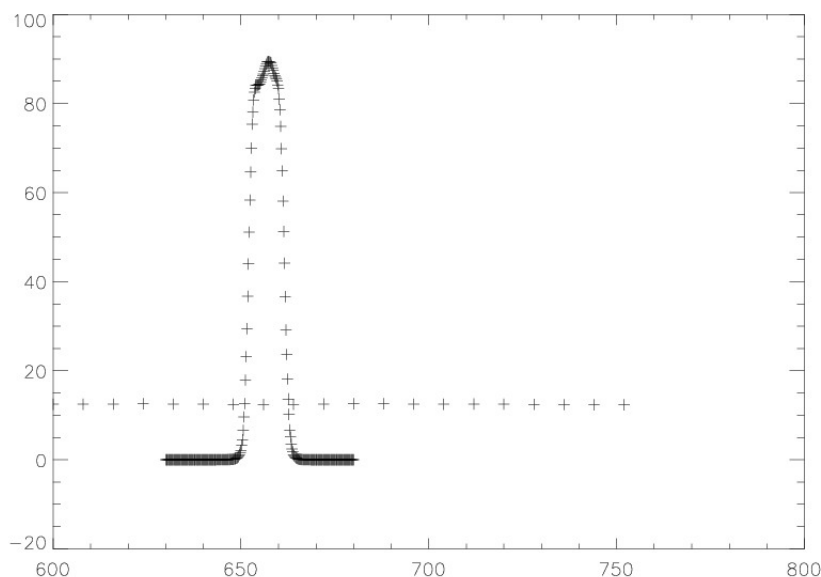


Figure 3.2.2: The spectrum of Feige 24 and the transmission curve of the Ha filter.

For example, if we measure the flux in ADUs from one nebula, now it's very easy to calculate its flux in  $erg/sec/cm^2$ . The only thing that we need to do is to multiply the flux in ADUs with the calibration factor (CF). But the WFC (Wide Field Camera of the INT) has 4 CCDs and every CCD has different response. So, we checked all CCDs and we found that the scale factor's differences in all CCDs do not differ by more than 5,1 % (Table 3.2.2)

Table 3.2.2: CCDs information

	CCD 1	CCD 2	CCD 3	CCD 4
CCD 1		4.63 %	5.04 %	4.60 %
CCD 2	4.63 %		0.63 %	4.28 %
CCD 3	5.04 %	0.63 %		2.06 %

These differences are very small. Because it is very difficult to have data from photometric nights only, we use the data from photometric nights to calibrate the data taken under non-photometric conditions. We took some information for the calibration factors from another project (Photometric atlas of NGC6822. Mislis, Zurita, Corradi). They estimate the flux from a star, or from a nebula and then calculate the new calibration factors for the rest of the nights. They measured the fluxes from two popular nebulas in NGC 6822. Hubble X and Hubble V in all filters. The results are presented in Table 3.2.4.

Table 3.2.3: Fluxes and CF in HX and HV

	Flux (ADU/sec)	erg/sec/cm <sup>2</sup>	New Calib.Factor
<b>H<math>\alpha</math>-filter</b>			
H-X (Phot)	7375.66	4.07906*10 <sup>-12</sup>	
H-X (non-Phot)	8945.39	4.07906*10 <sup>-12</sup>	5.53*10 <sup>-16</sup>
H-V (non-Phot)	10437.68	4.75953*10 <sup>-12</sup>	
<b>SII-Filter</b>			
H-X (Phot)	1174.48	2.49465*10 <sup>-13</sup>	2.12*10 <sup>-16</sup>
H-V (Phot)	928.138	1.97146*10 <sup>-13</sup>	
<b>He-Filter</b>			
H-X (Phot)	112.120	7.10779*10 <sup>-14</sup>	
H-X (non-Phot)	116.77	7.10779*10 <sup>-14</sup>	5.85*10 <sup>-16</sup>
H-V (non-Phot)	128.51	7.51089*10 <sup>-14</sup>	
<b>OIII-Filter</b>			
H-X (Phot)	6540.87	8.81451*10 <sup>-12</sup>	
H-X (non-Phot)	6567.90	8.81451*10 <sup>-12</sup>	1.35*10 <sup>-15</sup>
H-V (non-Phot)	8845.57	1.18713*10 <sup>-11</sup>	

These data are quite good if we compare them with previous papers like O'dell, Hodge & Kennicutt (1999), Kennicutt (1978), E.D. Skillman, R. Terlevich & J. Melnick (1989), Hidalgo - Gamez and Pagel, Edmunds & Smith (1980) (Table 3.2.5).

Also, we compare here some important line ratios measured by several authors with the line ratios obtained in this work for Hubble V and Hubble X.

#### HUBBLE X

Hidalgo - Gamez (2001)

$$\frac{H\alpha+NII}{SII} = 17.25 \pm 7.74$$

$$\frac{H\alpha+NII}{OIII} = 0.61 \pm 0.46$$

Pagel, Edmunds & Smith (1980)

$$\frac{H\alpha+NII}{SII} = 18.50$$

Corradi Romano, Zurita Almudena, Mislis Dimitris

$$\frac{H\alpha+NII}{SII} = 16.32 \pm 2.18$$

$$\frac{H\alpha+NII}{OIII} = 0.46 \pm 0.06$$

#### HUBBLE V

E.D. Skillman, R. Terlevich & J. Melnick (1989)

$$\frac{H\alpha+NII}{SII} = 22.45 \pm 2.18$$

$$\frac{H\alpha+NII}{OIII} = 0.47 \pm 0.03$$

Table 3.2.4: Comparison of Fluxes

	HV Flux ( $10^{-12} \text{erg/sec/cm}^2$ )	HX Flux ( $10^{-12} \text{erg/sec/cm}^2$ )
<b>CZM*</b>		
Ha 6568/95	$4.76 \pm 0.63$	$4.08 \pm 0.54$
OIII 5008/100	$11.9 \pm 0.26$	$8.81 \pm 0.19$
SII 6725/80	$0.20 \pm 0.004$	$0.25 \pm 0.005$
He 4686/100	$0.75 \pm 0.002$	$0.71 \pm 0.002$
<b>O' DELL, HODGE &amp; KENNICUTT (1999)</b>		
Ha	4.8	3.2
<b>KENNICUTT (1978)</b>		
Ha	5.2	4.0
<b>E.D. Skillman, R. Terlevich &amp; J. Melnick (1989)</b>		
Ha	2.92	
SII	0.13	
OIII	6.24	
<b>Pagel, Edmunds &amp; Smith (1980)</b>		
Ha	3.62	1.85
SII	0.19	0.10
OIII	8.15	

Pagel, Edmunds & Smith (1980)

$$\frac{Ha+NII}{SII} = 19.05$$

$$\frac{Ha+NII}{OIII} = 0.44$$

Corradi Romano, Zurita Almudena, Mislis Dimitris

$$\frac{Ha+NII}{SII} = 23.80 \pm 3.18$$

$$\frac{Ha+NII}{OIII} = 0.40 \pm 0.05$$

PNe

Dufour & Talet (1980)

$$\frac{He}{Ha+NII} = 0.06 \pm 0.008$$

$$\frac{He}{OIII} = 0.05 \pm 0.007$$

Corradi Romano, Zurita Almudena, Mislis Dimitris

$$\frac{He}{Ha+NII} = 0.07 \pm 0.008$$

$$\frac{He}{OIII} = 0.03 \pm 0.007$$

### 3.3 Construction of the HII regions catalogue

#### 3.3.1 Hot stars in IC10 and SexB

HII regions are highly ionized Hydrogen clouds. Near them there is always one (in small regions) or more maybe clusters, - (in large regions) hot stars. The radiation from these stars, ionize the enviroment of the regions, and the regions become bright. Of course is a function of the luminosity of each region the number of hot stars. So, the logic that we followed is simple: We tried locate to the hot stars in order to estimate the real number of smaller nebulas in the complicated regions (Figure 3.3.1 and 3.3.3). We detected the HII regions by plotting isophot contour lines at a pre-determined level, using the **F.O.C.A.S.** package of **IRAF**. The Faint Object Classification and Analysis System (**FOCAS**) is a set of programs for creating and manipulating catalogs of objects from digital astronomical images. The catalogs are created by an automatic threshold detector where the threshold is measured relative to a simultaneously determined background. The manipulation of catalogs includes the separation of merged objects, the measurement of various position, shape, and photometric parameters, the astronomical classification of the objects, matching of different catalogs of the same field, interactive display and review, and analysis operations using various tools and user written procedures. **FOCAS** may be used on any type of astronomical image data but it was primarily designed for the optimal detection of small faint objects and their classification as stars, galaxies, or noise. It is largely automated for the measurement of large numbers of objects for various statistical studies. It was not intended for very crowded stellar fields where point spread function fitting methods are more appropriate, or for large bright objects where surface brightness methods apply. Then, in order to identify the individual HII regions found in complex and blended regions, we seeked and studied the distribution of hot (blue supergiant) stars in the vicinity, selected by the Color-Color diagram (Figures 4.1.2 and 4.1.3). In subsequent observations extinction was ignored, without any significant effect in our results.

The hot stars in a galaxy, as we know, are the early spectral types O and B. We estimated the extinction of the interstellar matter in our Galaxy and we found that the hot stars in IC10 and Sextan B galaxies belong in a magnitude window between:  $16.1 < m < 20.6$ . We know that the difference in magnitudes of a star, in two colors is:

$$M_{red} - M_i = -2.5 * \log\left(\frac{I_i}{I_{red}}\right) + constant \quad (3.3.1)$$

Also we know that the color window about hot stars in filters r and i (sloan) is:

$$-0.45 < M_r - M_i < 0.15 \quad (3.3.2)$$

So,among the  $\sim 70000$  the stars in each galaxy we only need to select these stars that comply with equation 3.3.2. In order to find the magnitudes of the blue stars we used the **Daophot II** software and Point Spread Function *PSF* photometry.

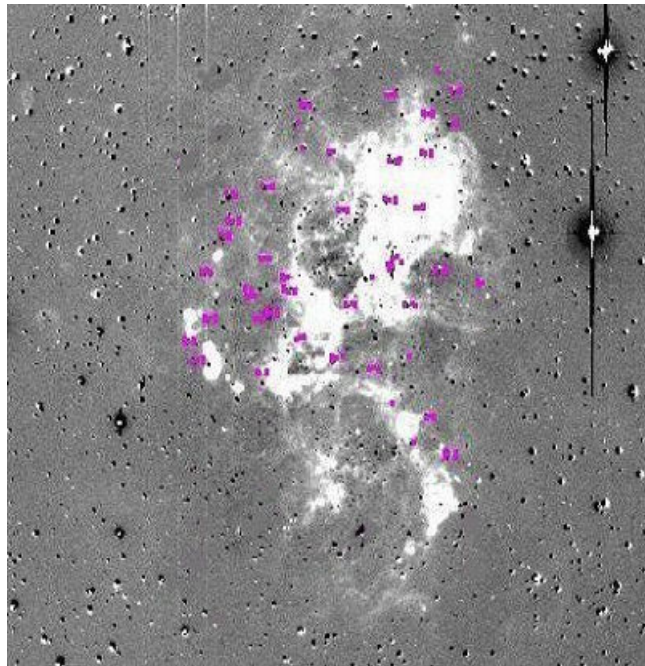


Figure 3.3.1: The blue stars in the IC10 galaxy.

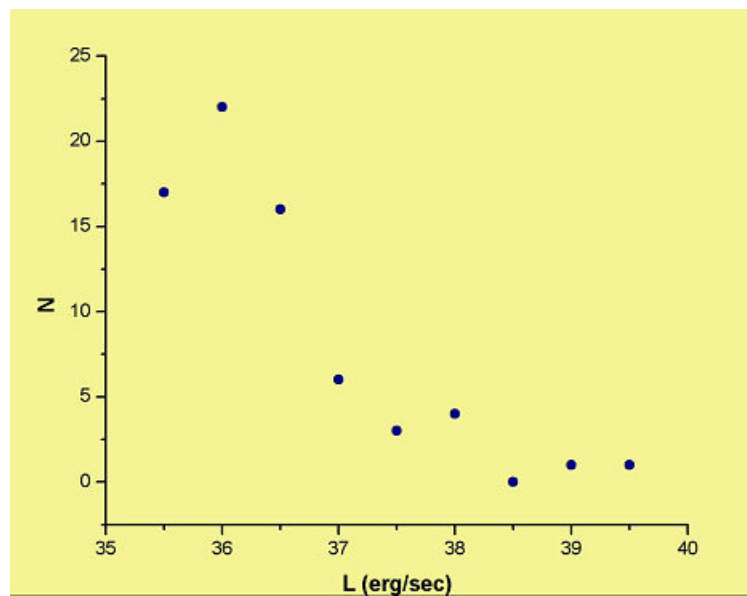


Figure 3.3.2: Luminosity Function in the IC10 galaxy.

### 3.4 FOCAS Software

In order to detect the HII regions with **FOCAS**, we need to create first an image catalogue (test.cat). We can do this with the command

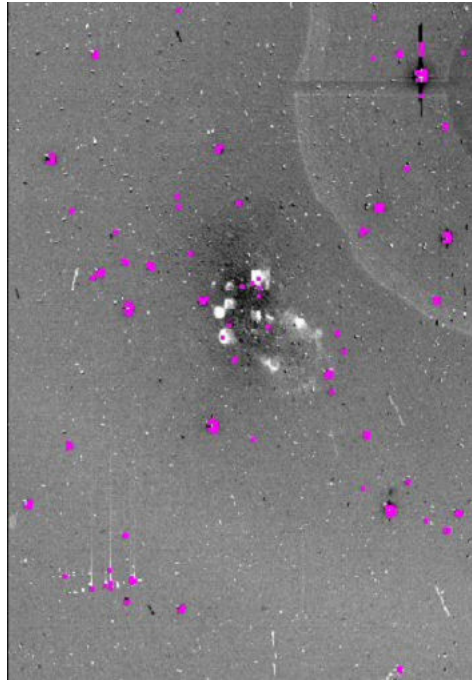


Figure 3.3.3: The blue stars in the Sextan B galaxy.

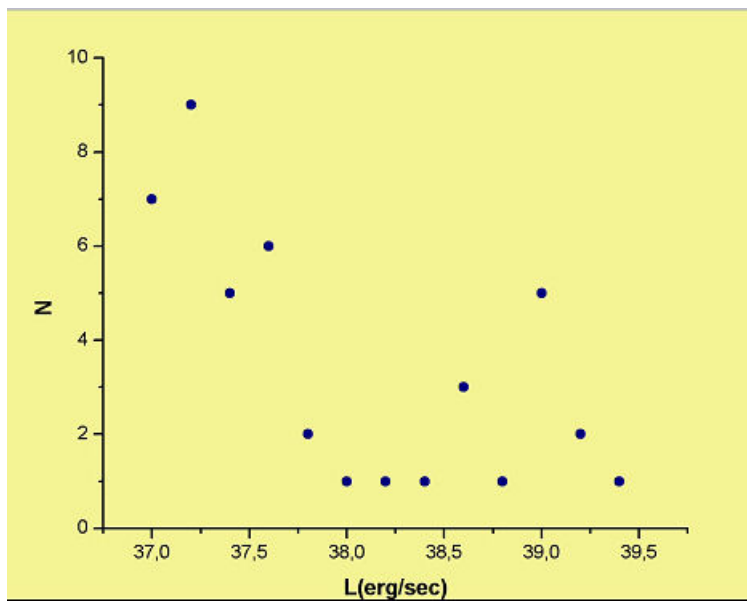


Figure 3.3.4: Luminosity Function in the Sextan B galaxy.

```
setcat
```

```
. For example:
```

```

fo> setcat test.cat

, [test.cat is the output file]

Set catalog header parameters? y
Field image file (): test
Field name : HII
Field epoch :
Field passband ():
Field coordinates in decimal (0. 0.):
Exposure or integration (0):
Observer ():
Origin (NOAO-\textbf{IRAF} FITS Image Ker):
Saturation value (): 60000
Magnitude zero point (): 30
Catalog magnitude limit (100.):
Radius of fixed circular aperature ():10
Sigma density above sky for detection (2.5):
Sigma density below sky for detection ():3
Sigma of sky (0 = automatic determination) (0.):
Minimum area for detection (6):
Significance level for evaluation and splitting (-100.):
Area description filename (test.ar):
Sky updating constants (0.1 0.1):
Comments:
  Thu 14:30:39 18-Mar-20: setcat
  Additional comments (Exit with $$ cr> or EOF):

Set detection filter? y
Use builtin filter? y
Set coordinate transformation?
Set intensity relation?
Set point spread function?
Set classification rules?

```

when this process is finished the catalogue file is created. This is a very important file. Now we are ready to detect the HII regions, perform, sky correction and evaluate. We type:

```

fo> detect test.cat (The extension of new file MUST be *.cat)
fo> sky test.cat
fo> evaluate test.cat
fo> filters test.cat new.cat [new.cat is the output file]
then we can select the filters. For example we used
M 0 20 G BD

```

**eflgs** is a 16 bit word whose bits represent various **flags**. The currently defined **flags** are given in Table 3.4.1. The first column is the variable name and the second column gives the filter option identifier. We set these parameters because, M 0 20 means we want only the regions with intensities 0 to 20 G BD means we

want only the regions without these flags B edge of the frame, D dark region. After these commands we can take some results. If we open now **ximtool**, the **IRAF** image display window, and type:

```
fo> review test.cat
```

we can see the image in the **ximtool** screen and in **IRAF** screen we have this commands:

```

                                FOCAS IMAGE REVIEW

test.cat
HII
  0.0          Class: u          Scale = 0.00          Fraction = 0.00
x: 1857.0      y: 1443.0         RA = 1857.0000       DEC = 1443.0000
Core = -5.55   Aperture = -6.29     Isophotal = -5.63   Total = -6.23
r1 = 0.93     r2 = 1.17             r3 = 1.30           r4 = 1.41
Area = 4      Sky = -2.78       Isophote = -4.13    Flags: ----B----E

Filter:
Command:

# catalog [1-4]      cursor select  a set class      b set flags
c continue          d set display  e evaluate        f set filter
y redraw terminal z zoomview sizes : shell command  T write textoff

```

With the letter 'h' FOCAS draws the isophots curves in the image. If we are happy with that we continue. If not we change the values of the 'Minimum area detection' and the 'Significance level for evaluation'. If the isophots are satisfactory, we press 'k' to see the object, and we check the *Flags*. The *Flags* have the most useful information. The meaning of these *Flags* are given in Table 3.4.1

With button 'n' we can see all the object and with the button 'i' erase the region. We selected only the 'E' objects. To find the fluxes of these object we need some calculations. We wrote a simple **FORTTRAN** code (**PHOT**) to make all these calculations. This code uses the equation 3.4.1 as the basic equation.

$$FLUX_1 = 10^{\frac{m_{zeropoint} - m_{total}}{2.5}} \quad (3.4.1)$$

$$FLUX = \frac{FLUX_1}{Time_{exp}} \quad (3.4.2)$$

Table 3.4.1: Flags in FOCAS

A	General use Flag to signal spacial attention
B	Object touches the edge of the field
C	The resolution classifier had problems
D	The object is below the sky
E	The object was successfully evaluated
F	The object has had a forced classification
L	Object exceeds the current limits of FOCAS
P	There are saturated pixels in the object
R	This object is a coordinate reference point
S	The object not split at any level by <i>Splits</i>

The zero point magnitude is the same zero point as the catalogue file and the total magnitude is the result from evaluation. After using the equations 3.4.1 and 3.4.2 we have the fluxes in ADUs/sec. Then the **PHOT** code can estimate which from these regions, exceed  $3\sigma$ .  $\sigma$  is evaluated from the sky value. Also, the information 'Area' which we take from **FOCAS** is very useful. We know the area of every region and then it is especially easy to calculate the radius of every region using the **FOCAS** s/w. We did this for all filters. As we have already said the from Ha detection with **FOCAS** software we create a image.cat and a image.ar files tha **FOCAS** used for the detection. The image of every region has the same name in all filters (for example image.fit in Ha, SII, OIII, He). Then we copy the .cat and .ar files in other filters and run **FOCAS** again. With button 'e' we estimate the flux again in other filters. After that we have the fluxes in all filters and the photometric catalogue.

### 3.5 Astrometry

One of the most interesting elements in the Photometric Atlas is the Astrometry of the HII regions, in each galaxy. In order to do this used the package **IRAF**. The data from the INT have some astrometry calibration, but we need to complete the **IRAF** scripts with some values. To have the right coordinary system we need to type:

```
cl> epar imexa
wcs =      world
xformat = $\%$H
yformat = $\%$H
```

**IRAF** use the ZPX coordinate system, and **GAIA** for example use the ZPN. **IRAF** understands another projection called ZPX which is almost equivalent to ZPN but it is not standard. One possibility is therefore to convert the WCS [World Coordinate System in FITS] in the FITS headers from ZPN to ZPX. If

### 3.5. *ASTROMETRY*

37

we want to pass from one system to the other for the Right Ascension we can type the following script in **IRAF**:

```
hedit FRAME ctype1 'RA---ZPN' ver+
FRAME,CTYPE1 (RA---ZPX -> RA---ZPN): y
FRAME,CTYPE1: RA---ZPX -> RA---ZPN
update FRAME ? (yes): yes
FRAME update
```

and the same for Declination:

```
hedit FRAME ctype2 'DEC---ZPN' ver+
FRAME,CTYPE2 (DEC---ZPX -> DEC---ZPN): y
FRAME,CTYPE2: RA---ZPX -> RA---ZPN
update FRAME ? (yes): yes
FRAME update
```

And the Astrometry is done! From now on every pixel on the image has the correct coordinates.



# Chapter 4

## Results

### 4.1 IC 10 and Sextan B

We have detected 70 HII regions in IC 10 and 44 HII regions in Sextan B. In Tables 4.1.1-4.1.7 we summarize the basic characteristics of each region. In particular, we present the  $H\alpha$  and  $OIII$  spectral line fluxes in IC 10 and the  $H\alpha$ ,  $OIII$  and  $SII$  in Sextan B. Furthermore we give  $f(r)$  of each region for both galaxies. The space occupied by a region is a logarithmic function of the flux density, obeying  $\log S \sim \log(r_3)$  (4.1.1), where S stands for the flux density and r stands for the radius of the region (Figures 4.1.4 and 4.1.5).

We know that Hydrogen in order to be ionized needs less energy than Sulphur, Oxygen or Helium. So the first element to be ionized in big quantities is Hydrogen because the stars with spectral types O and B can easily emit photons with energies 13.6 - 24.6 eV. The energy of ionization in sufficient quantities for HeII is  $E = 54.4$  eV, which is too high for the stars of this type to emit. Thus minimal HeII exists in these regions. Similar phenomena are also observed in the other elements. For example the map of  $H\alpha$  and  $SII$  is characteristic.

From the measurements that we made we could estimate the luminosity and the radius of every HII region in the two galaxies under investigation. Let's suppose that in these regions prevails the Hydrogen. This means that its density will be of the order of  $\rho_H = 1.6726 \times 10^{-21} \text{ kg/m}^3$ . From the equation of mass we can easily calculate for constant density that

$$M = \frac{4}{3} \pi R^3 \rho_H \quad (4.1.2)$$

The temperature of the HII clouds is also very useful quantity. Therefore we will try to calculate it using our observations. The temperature of an ideal gas is given by:

$$T = \frac{2\pi G m_\rho \mu_\rho R^2}{3\kappa_B} \quad (4.1.3)$$

In order to calculate the mass and the temperature of each region we created two simple fortran codes. These calculations are presented in Tables 4.1.8, 4.1.9 and 4.1.10. Having calculated the temperature of the clouds we can use the virial theorem to estimate the minimum mass that the clouds should have in order to begin gravitation contraction. Therefore assuming that the dynamic

energy should be higher than the internal energy of the clouds (in order to begin contraction), the minimum (or the critical) mass  $M_c$  should be :

$$M_c > 5k_B R_c T / G m_\rho \mu \quad (4.1.4)$$

In some regions we find that the critical mass is larger than the real mass of the cloud. This result could be very interesting. If we assume that this extra mass can be attributed to the constant radiation of the ionizing star of the cloud we will have

$$\Delta M = M_{crit} - M_{real} \quad (4.1.5)$$

However the rate of the change of energy is equal to the luminosity of the cloud. That is to say

$$dE/dt = L \quad (4.1.6)$$

hence

$$c^2 dM/dt = L \quad (4.1.7)$$

Consequently we can make an estimation of the star found in the centre of the cloud. This is that radiates and loses mass which in turns becomes luminosity generally is in effect that

$$M_\alpha = M_\beta + M_\gamma \quad (4.1.8)$$

where  $M_\alpha$  stands for the mass which the cloud had before, where  $M_\beta$  stands for the mass that cloud has now and where  $M_\gamma$  stands for the mass of the star. Finally the Figures 4.1.4 and 4.1.5 have great interest. These give the diagrams of logarithm of luminosity and logarithm of third force of the radius of the respective region in each galaxy. We also observe from the Figures that a linear equation between these two sizes should be. This is important for the following reason. It is obvious that the luminosity with the mass is generally linear function in the regions of Hydrogen as long as more material is ionized by the central star so much more the energy is which is radiated by the cloud. Since we have proved that the luminosity is linear with the third force of the radius hence an acknowledgement will be supposed to exist that we made in the beginning of our study. That density of the clouds of Hydrogen is roughly constant.

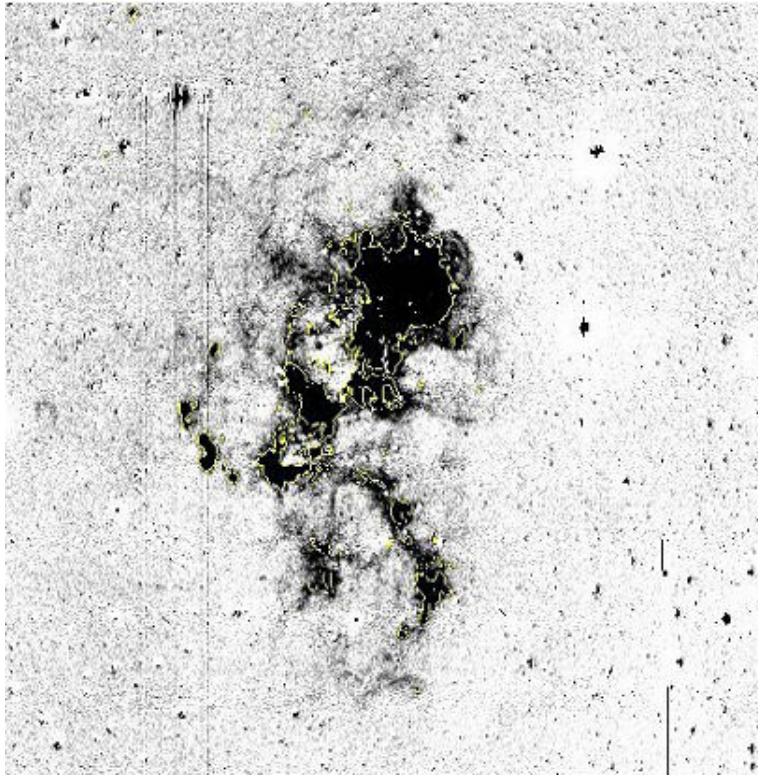


Figure 4.1.1: IC10.

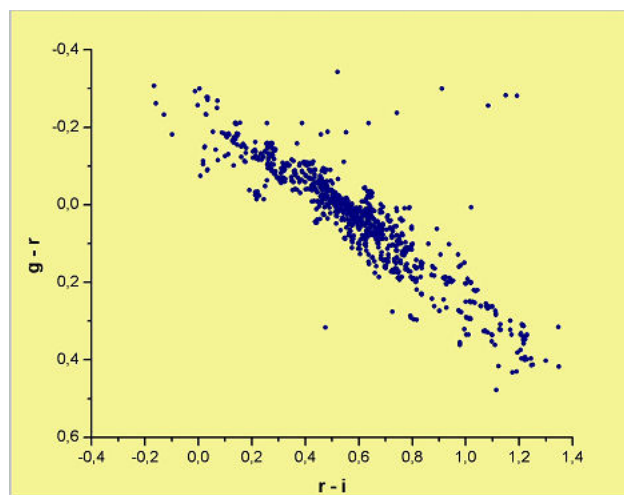


Figure 4.1.2: Color - Color diagram of the IC 10 galaxy.

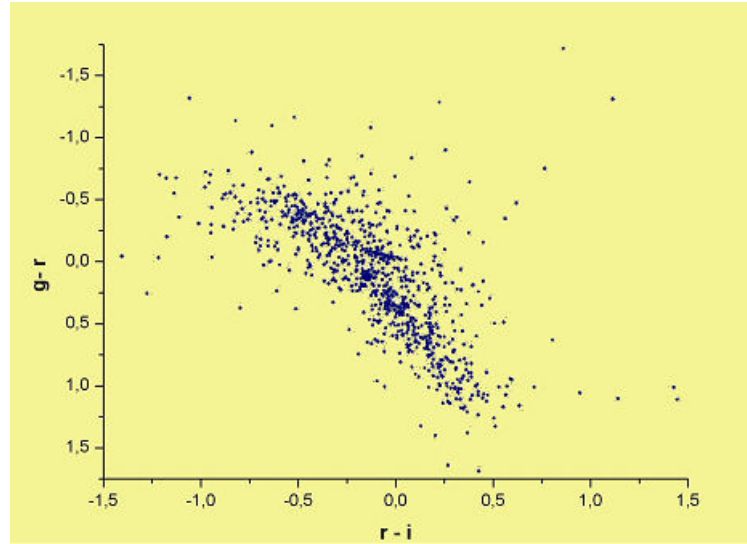


Figure 4.1.3: Color - Color diagram of the Sextan B galaxy.

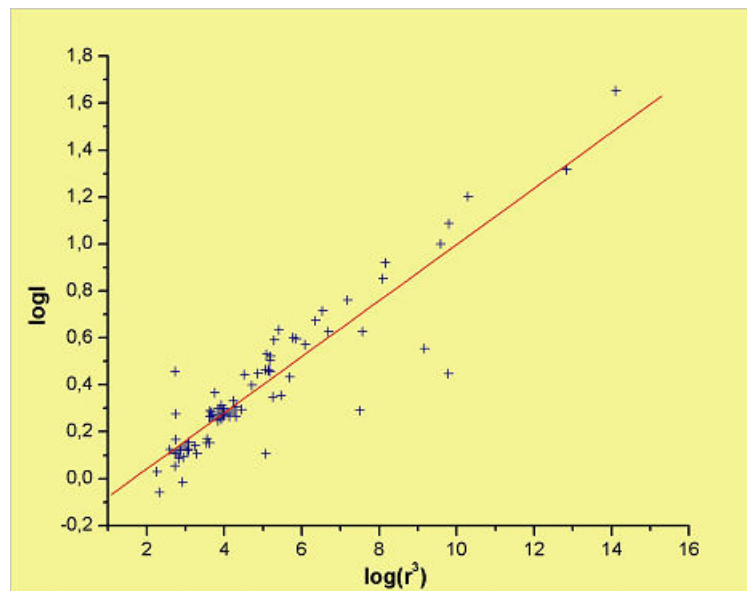


Figure 4.1.4: Luminosities vs Radius of HII regions in IC 10 galaxy.

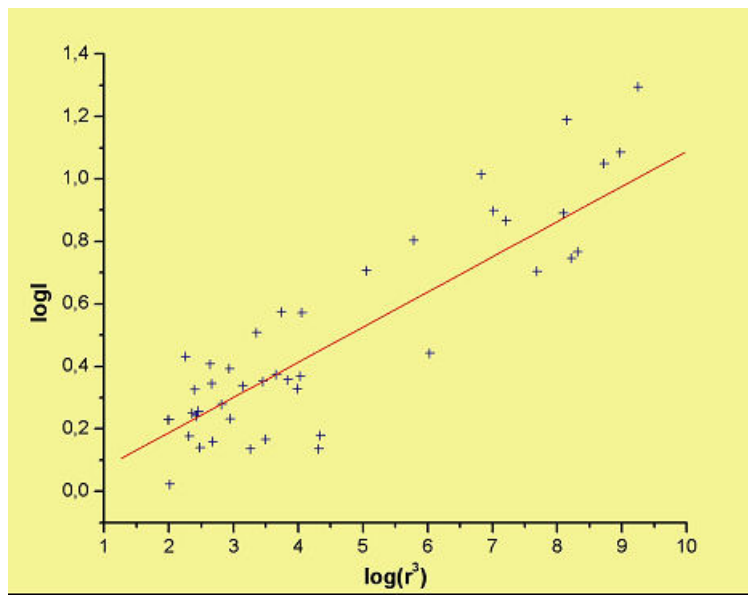


Figure 4.1.5: Luminosities vs Radius of HII regions in Sextan B galaxy.

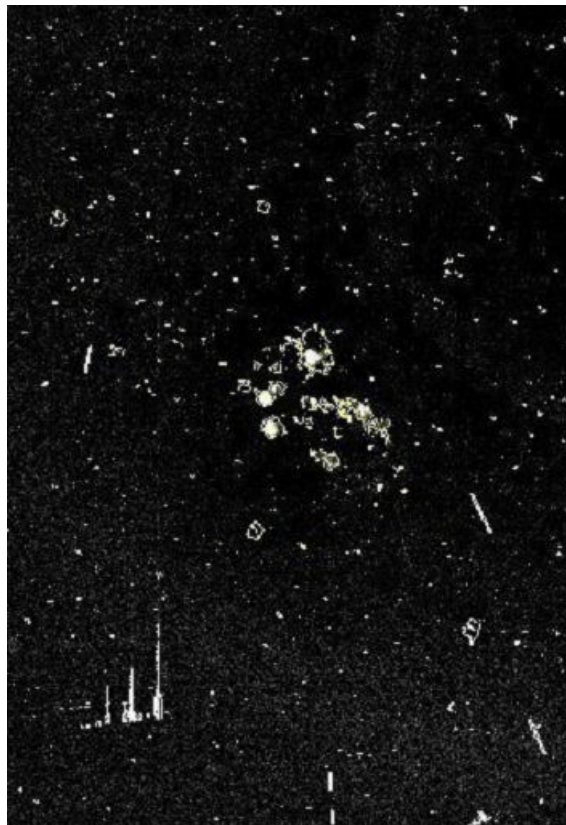


Figure 4.1.6: Sextan B.

Table 4.1.1: IC 10 objects

IC 10 Objects				
Name	Flux in Ha ( $10^{-16}$ erg/sec/cm $^2$ )	Flux in OIII ( $10^{-16}$ erg/sec/cm $^2$ )	Flux in SII ( $10^{-16}$ erg/sec/cm $^2$ )	Radius (arcsec)
50	379.162	7.76	274.73	
372	25.445	5.09		
401	297.297	7.07	107.32	1.27
461	266.897	5.55		
486	250.620	3.81		
569	242.481	5.41		
600	254.929	4.70		
630	30.400	7.63	91.85	4.30
634	257.801	5.78		1.43
654	268.573	5.81		1.94
660	24.128	6.11	93.77	1.06
667	270.967	6.49	92.12	2.33
672	272.642	6.51	94.69	1.76
691	309.505	7.01	91.85	2.70
772	317.644	7.37	99.91	3.73
774	257.083	6.29	83.97	
790	26.929	6.89	98.81	1.91
799	247.987	5.07		1.32
801	2.805	7.18	106.32	2.14
813	29.969	7.48	107.42	3.31
824	250.620	7.42	133.06	2.86
828	260.913	6.25	105.03	1.38
846	274.557	6.80	106.5	2.05
847	29.777	7.25	103.39	3.38
863	269.770	6.68	90.38	
868	278.626	6.56	98.35	1.84
872	253.492	6.26	88.55	
873	298.733	7.17	101.5	2.90
893	339.426	7.62	116.85	5.77
902	28.485	7.05	95.33	1.97
906	347.086	7.85	118.31	4.22
911	275.754	6.81	83.42	
926	290.116	7.31	95.78	2.49
942	293.228	7.02	91.21	
987	250.620	5.97	91.85	1.27
1002	257.562	5.46		1.32
1026	272.642	6.22	116.30	1.98
1029	252.535	6.25	93.13	1.22

Table 4.1.2: IC 10 objects

IC 10 Objects				
Name	Flux in Ha ( $10^{-16}$ erg/sec/cm <sup>2</sup> )	Flux in OIII ( $10^{-16}$ erg/sec/cm <sup>2</sup> )	Flux in SII ( $10^{-16}$ erg/sec/cm <sup>2</sup> )	Radius (arcsec)
1071	275.275	6.94	96.43	1.89
1083	357.618	7.99	131.23	7.12
1100	275.754	6.71	91.21	
1104	268.333	4.84		
1109	268.333	6.63	115.66	1.83
1124	345.650	8.32	140.29	1.95
1127	305.196	6.79	99.91	2.26
1128	261.870	5.33		
1134	452.170	1.06	143.31	20.73
1155	300.888	6.46	90.75	
1158	387.300	9.13	142.12	10.01
1159	311.420	7.33	120.24	3.98
1177	299.452	6.94	107.87	3.17
1179	301.606	6.75	109.89	3.89
1180	329.612	7.44	93.31	4.23
1181	281.978	6.05	100.46	2.02
1192	401.423	9.46	127.93	15.93
1258	358.815	7.77	121.33	8.31
1317	274.557	6.91	114.28	1.79
1318	286.286	6.35	108.61	2.77
1322	250.859	3.88		1.89
1335	326.500	7.33	106.5	5.20
1340	250.859	5.74		
1361	391.370	6.45	108.519	2.80
1363	281.978	5.75		
1365	297.058	6.57	103.94	2.90
1412	322.910	7.27	109.89	4.72
1417	299.452	6.21	98.62	2.86
1479	391.609	8.73	129.85	12.23
1515	313.096	6.32	110.35	3.94
1645	267.137	5.83		
1033	477.543	1.13	166.57	44.92

Table 4.1.3: Sextan B objects

Sextan B Objects					
Name	Flux in Ha ( $10^{-16} \text{ erg/sec/cm}^2$ )	Flux in OIII ( $10^{-16} \text{ erg/sec/cm}^2$ )	Flux in SII ( $10^{-16} \text{ erg/sec/cm}^2$ )	Flux in HeII ( $10^{-16} \text{ erg/sec/cm}^2$ )	Radius (arcsec)
1703	1444.28	31.94	491.94		2.768
1708	1288.05	30.66	547.11		1.368
1825	1632.19	40.89	705.93	1973.16	7.766
1923	1163.50				1.706
1994	1209.39	28.07	527.88	1297.73	2.250
2148	1655.13	37.66	645.33	1585.22	1.303
2183	1257.46	30.32	454.74	1261.94	2.131
2338	1516.38	33.60	562.16	1469.76	1.035
2577	1118.71		472.71	1169.58	1.805
2599	1200.65		485.25	1243.47	3.225
2606	1076.10	27.91			1.696
2685	1235.61	33.81	487.34	1384.33	3.757
2689	1135.10	30.32	461.84	1286.19	2.553
2704	1689.00	37.74	583.89	1489.39	1.118
2717	1078.29				1.053
2852	1191.91	27.81	462.68		1.368
2862	1421.33	34.45	534.99	1468.61	6.359
2894	1533.8	36.19	562.57	1526.34	7.914
3054	1120.90				1.381
3055	1711.94	40.59	598.10	1542.50	1.215
3075	1105.60				1.501
3076	1244.35	29.94	653.27	1340.45	2.273
3078	1651.8	39.02	664.97	1823.06	5.847

Table 4.1.4: Sextan B objects

Sextan B Objects					
Name	Flux in Ha ( $10^{-16}$ erg/sec/cm <sup>2</sup> )	Flux in OIII ( $10^{-16}$ erg/sec/cm <sup>2</sup> )	Flux in SII ( $10^{-16}$ erg/sec/cm <sup>2</sup> )	Flux in HeII ( $10^{-16}$ erg/sec/cm <sup>2</sup> )	Radius (arcsec)
3267	1354.69	33.71	512.4	1417.8	5.096
3281	1290.23	30.34	494.45	1214.60	1.512
3282	1138.38		440.95		1.442
3301	1264.01		485.67	1273.49	3.733
3324	1116.53				1.746
3375	1212.67	30.82	478.98	1177.66	1.466
3490	1595.0	27.14	644.49	1693.75	5.065
3501	1162.41	27.30	427.99	1179.97	2.470
3505	1100.14	30.45	467.28	1281.57	2.698
3510	1227.96	26.93	665.39	1310.43	2.370
3576	1109.97		595.17	1211.1	1.776
3722	1137.28	26.87	461.01		2.211
3762	1737.07	41.34	631.12	1719.15	19.70
4142	1151.49		555.47	1511.33	1.899
4281	1077.2	27.49			1.696
4480	1180.98		510.75	1252.70	2.171
4848	111.32	28.61	446.38		2.115
5093	1551.34	42.09	690.47	1962.77	7.369
5174	1643.11	38.24	663.30	1818.44	5.574
5184	1261.8	28.72	655.78	1631.40	2.333
2901	1131.82		451.81	1237.69	2.526
2878	1636.5	35.84	599.35	1545.97	15.45

Table 4.1.5: IC 10 Astrometry

IC 10 Astrometry		
Name	Right ascension	Declination
50	00:20:53.891	+59:21:08.19
372	00:20:44.525	+59:18:37.96
401	00:20:44.103	+59:19:09.71
461	00:20:40.508	+59:21:33.55
486	00:20:40.321	+59:17:20.58
569	00:20:36.600	+59:16:54.23
600	00:20:35.257	+59:18:05.64
630	00:20:34.027	+59:17:16.13
634	00:20:33.733	+59:17:06.75
654	00:20:32.560	+59:17:58.35
660	00:20:44.171	+59:17:56.78
667	00:20:32.117	+59:18:08.34
672	00:20:31.712	+59:18:23.32
691	00:20:31.177	+59:18:10.65
772	00:20:27.844	+59:18:20.27
774	00:20:27.355	+59:18:03.97
790	00:20:26.712	+59:18:04.88
799	00:20:25.917	+59:18:47.28
801	00:20:26.063	+59:18:07.10
813	00:20:25.715	+59:18:55.59
824	00:20:25.435	+59:18:19.14
828	00:20:24.383	+59:18:16.75
846	00:20:23.555	+59:18:57.52
847	00:20:23.731	+59:18:34.28
863	00:20:22.829	+59:18:12.83
868	00:20:22.915	+59:19:02.58
872	00:20:22.507	+59:17:13.13
873	00:20:22.931	+59:17:08.10
893	00:20:22.655	+59:16:34.93
902	00:20:21.438	+59:17:19.90
906	00:20:22.150	+59:20:02.35
911	00:20:43.341	+59:18:06.84
926	00:20:21.525	+59:18:09.67
942	00:20:20.256	+59:18:26.42
987	00:20:18.384	+59:17:05.32
1002	00:20:17.902	+59:16:14.86
1026	00:20:16.982	+59:20:19.57
1029	00:20:16.475	+59:19:06.95

Table 4.1.6: IC 10 Astrometry

IC 10 Astrometry		
Name	Right ascension	Declination
1071	00:20:20.810	+59:17:31.59
1083	00:20:15.104	+59:18:52.07
1100	00:20:16.464	+59:20:27.49
1104	00:20:13.769	+59:19:57.21
1109	00:20:13.791	+59:19:57.36
1124	00:20:13.380	+59:18:57.11
1127	00:20:12.456	+59:18:26.22
1128	00:20:12.135	+59:18:48.06
1134	00:20:11.894	+59:17:37.65
1155	00:20:17.405	+59:18:39.82
1158	00:20:10.800	+59:19:56.75
1159	00:20:12.853	+59:20:10.39
1177	00:20:10.729	+59:18:25.89
1179	00:20:10.214	+59:18:34.70
1180	00:20:09.807	+59:17:52.80
1181	00:20:09.719	+59:19:47.17
1192	00:20:09.154	+59:17:57.16
1258	00:20:10.065	+59:19:13.88
1317	00:20:07.182	+59:17:25.13
1318	00:20:03.416	+59:16:50.69
1322	00:20:04.485	+59:17:20.60
1335	00:20:03.456	+59:17:34.64
1340	00:20:03.531	+59:18:39.69
1361	00:20:02.696	+59:18:16.84
1363	00:20:03.421	+59:16:50.73
1365	00:20:01.237	+59:16:40.68
1412	00:20:01.059	+59:17:03.95
1417	00:20:00.405	+59:18:27.13
1479	00:20:01.214	+59:18:38.59
1515	00:19:58.637	+59:16:40.95
1645	00:19:54.716	+59:17:21.89
1033	00:19:49.346	+59:17:11.31

Table 4.1.7: Sextan B Astrometry

Sextan B Astrometry		
Name	Right ascension	Declination
1703	10:00:11.289	+05:19:26.23
1708	10:00:10.882	+05:16:58.80
1825	10:00:10.123	+05:20:18.23
1923	10:00:08.089	+05:18:11.04
1994	10:00:07.181	+05:17:40.62
2148	10:00:05.854	+05:17:48.82
2183	10:00:05.496	+05:17:44.89
2338	10:00:04.973	+05:19:03.73
2577	10:00:02.802	+05:17:04.11
2599	10:00:03.409	+05:18:55.70
2606	10:00:02.805	+05:19:23.71
2685	10:00:02.274	+05:19:26.46
2689	10:00:02.852	+05:19:35.08
2704	10:00:02.744	+05:20:06.25
2717	10:00:01.995	+05:19:50.66
2852	10:00:00.810	+05:18:22.90
2862	10:00:01.194	+05:19:06.71
2894	10:00:01.718	+05:18:50.24
3054	10:00:00.847	+05:19:20.06
3055	10:00:00.654	+05:18:56.16
3075	09:59:59.518	+05:19:28.26
3076	10:00:00.858	+05:20:10.09
3078	09:59:59.536	+05:22:16.95
3267	09:59:59.473	+05:20:36.04
3281	09:59:59.914	+05:20:30.65
3282	09:59:58.293	+05:19:59.04
3301	09:59:58.330	+05:20:56.16
3324	09:59:58.622	+05:20:43.41
3375	09:59:58.469	+05:20:16.11
3490	09:59:57.952	+05:22:01.05
3501	09:59:57.870	+05:22:54.39
3505	09:59:57.509	+05:22:46.49
3510	09:59:57.127	+05:20:12.08
3576	09:59:56.956	+05:19:53.94
3722	09:59:57.332	+05:22:47.85
3762	09:59:56.671	+05:21:45.59
4142	09:59:55.916	+05:21:39.74
4281	09:59:58.363	+05:19:29.78
4480	09:59:53.642	+05:17:09.57
4848	09:59:53.181	+05:23:33.67
5093	09:59:51.764	+05:16:57.89
5174	09:59:49.393	+05:22:13.38
5184	09:59:48.031	+05:23:49.13
2901	09:59:47.088	+05:20:12.85
2878	09:59:46.735	+05:20:18.23

Table 4.1.8: Temperature and mass of HII regions in IC 10 galaxy

IC 10		
Name	Temperature (Kelvin)	Mass ( $\times 10^{42} \text{kg}$ )
50	2.29686872	2.48515097x10
372	0.167157614	4.87907761
401	0.290977947	1.12056909
461	0.359079201	1.53615107
486	0.229067796	7.82698645
569	0.136202476	3.58860793
600	0.272404983	1.01501186
630	3.31219717	4.30350977
634	0.365270303	1.57605023
654	0.674821215	3.95759779
660	0.204303714	6.59269384
667	0.97199039	6.84134485
672	0.557192046	2.9693123
691	1.30630543	1.06589793
772	2.48879093	2.80305196
774	0.309551068	1.22955231
790	0.656248251	3.79534043
799	0.31574217	1.26662318
801	0.82340574	5.33420079
813	1.96255387	1.96282185
824	1.46108121	1.26084018
828	0.340506237	1.41852224
846	0.75530458	4.68631765
847	204.922.824	2.09427642
863	0.625293207	3.52999505
868	0.606720118	3.37389144
872	0.309551068	1.22955231
873	1.50441821	1.31735067
893	5.9433795	1.03442432
902	0.693394429	4.12210509
906	3.18837625	4.06446016
911	0.705776384	4.23300908
926	1.11438384	8.39848052
942	1.41155302	1.19727603
987	0.290977947	1.12056909
1002	0.31574217	1.26662318
1026	0.705776384	4.23300908
1029	0.266213912	9.80606308

Table 4.1.9: Temperature and mass of HII regions in IC 10 galaxy

IC 10		
Name	Temperature (Kelvin)	Mass (x $10^{42} kg$ )
1071	0.637675287	3.63536388
1083	9.06984703	1.95006233
1100	0.612911064	3.42566357
1104	0.359079201	1.53615107
1109	0.600529171	3.32238299
1124	0.681012411	4.01218607
1127	0.916271185	6.26158916
1128	0.290977947	1.12056909
1134	76.7562936	4.80086513
1155	0.885316016	5.94697347
1158	17.8982428	5.40585177
1159	2.83548793	3.40871137
1177	1.80158739	1.72636072
1179	2.7116675	3.18788884
1180	3.19456682	4.07630346
1181	0.730540482	4.45774216
1192	45.3182783	2.17800391
1258	12.3387047	3.09423198
1317	0.575764948	3.11900714
1318	1.37440672	1.15032726
1322	0.637675287	3.63536388
1335	4.82899616	7.57589325
1340	0.38384333	1.69777265
1361	1.40536182	1.18940774
1363	0.606720118	3.37389144
1365	1.51060953	1.32549124
1412	3.98701745	5.68356362
1417	1.46108121	1.26084018
1479	26.7142624	9.85742066
1515	2.77976854	3.30873134
1645	0.39003437	1.73901293
1033	360.224583	4.88099715

Table 4.1.10: Temperature and mass of HII regions in Sextan B galaxy

Sextan B		
Name	Temperature (Kelvin)	Mass ( $\times 10^{33} \text{kg}$ )
1703	6.24460464	1.11405325
1708	1.52583105	0.13455759
1825	49.137401	24.5904675
1923	2.37351453	0.261057615
1994	4.12539482	0.5982005
2148	1.38455049	0.116308577
2183	3.7.155249	0.508422077
2338	87.961902	58.3293686
2577	2.65607591	0.309036136
2599	8.47683822	1.7619735
2606	2.34525866	0.256409794
2685	11.5002463	2.78425622
2689	5.3121513	0.874085963
2704	101.976369	73.5186996
2717	0.904196215	0.0613822117
2852	1.5583105	0.13455759
2862	32.9466468	13.5009813
2894	51.030575	26.0252075
3054	1.55408745	0.138312578
3055	120.286336	94.1830978
3075	1.83664831	0.177700043
3076	4.21016297	0.616732597
3078	27.8605409	10.4986353
3267	21.1638365	6.95088577
3281	1.86490445	0.181816548
3282	1.69536762	0.157595694
3301	11.3589638	2.73310685
3324	2.48653935	0.279924899
3375	1.75188016	0.165540829
3490	20.9095347	6.82598066
3501	4.97307922	0.791747332
3505	5.93378581	1.03192079
3510	4.57749224	0.699181557
3576	2.57130802	0.294360608
3722	3.98411413	0.567735672
3762	316.383871	401.763092
4142	2.93863781	0.359639674
4281	2.34525866	0.256409794
4480	3.84283318	0.537806213
4848	3.64504021	0.496823341
5093	44.2490936	21.0138245
5174	25.3174912	9.09451485
5184	4.43621181	0.667063117
2901	5.19912675	0.84633863
2878	194.684752	

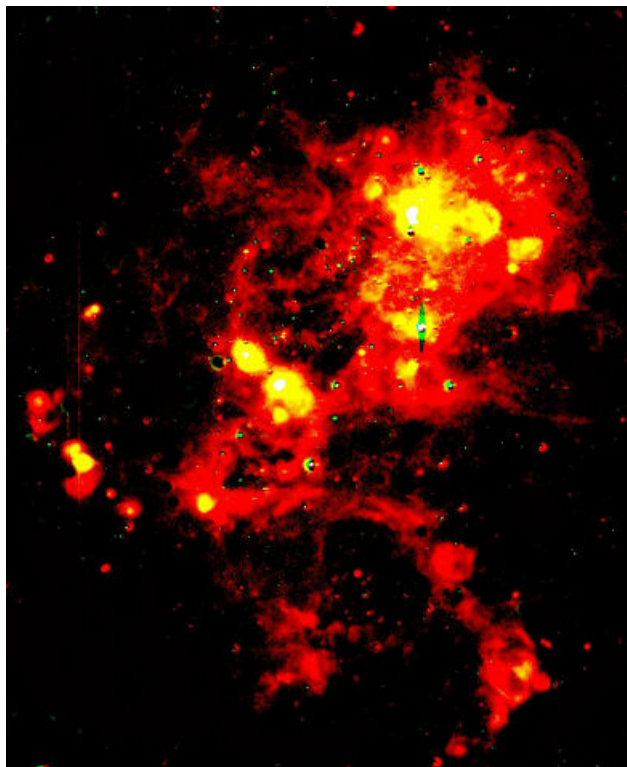


Figure 4.1.7: Color-Color map of IC 10.

# Bibliography

## THE PAPERS

- [1] G. Catanzaro, L. Bianchi, S. Scuderi & A. Manchado 2003, *A&A*, 403, 111-117
- [2] R. Corradi, A. Zurita, D. Mislis, NGC6822 Photometric Atlas Of HII Regions
- [3] R.J Dufour & D. L. Talent 1980, *ASJ*, 235, 22-29
- [4] E.L. Fitzpatrick 1999, *PASP*, 111, 63-75
- [5] R. Greimel, N.A. Walton, D.C Abrams, M.J Irwin, & J.R. Lewis, 2001, *ASP Conf. Ser.* 238
- [6] A.M. Hidalgo-Gamez, K. Olofsson & J. Masegosa 2001, *A&A*, 367, 388-404
- [7] Paul Hodge, R.C. Kennicutt, JR & Myung Cyoon Lee 1988, *PASP*, 100, 917-934
- [8] Paul Hodge, R.C. Kennicutt, JR & Myung Cyoon Lee 1989, *PASP*, 101, 32-39
- [9] Paul Hodge, R.C. Kennicutt, JR & Myung Cyoon Lee 1994, *AJSS*, 92, 119-123
- [10] P. Massey, T.E. Armandroff, R. Pyke, K. Patel & C.D. Wilson, 1995, *ASJ*, 110, 2715-2738
- [11] C.W. McAlary, B.F. Madore, R. McGonegal, R.A. McLaren & D.L. Welch 1983, *ASJ*, 273, 539-543
- [12] J.G. Nollenberg, E.D. Skillman, D.R. Garnett & H.L. Dinerstein 2002, *ASJ*, 581, 1002-2002
- [13] C.R O'Dell, P.W. Hodge & R.C Kennicutt 1999 *PASP*, 111, 1382-1392
- [14] B.E.J. Pagel, M.G. Edmunds & G. Smith 1980, *MNRAS*, 193, 219-230
- [15] M.S. Portal, A.I. Díaz, R. Terlevich, E. Terlevich, M.A .Alvarez & I. Aretxaga 2000, *MNRAS*, 312, 2-32
- [16] E.D. Skillman, R. Tilverich, J. Melnick 1989, *MNRAS*, 240, 563-572

- [17] R. Terlevich, M.S. Portal, A. I. Díaz & E. Terlevich, MNRAS, 249, 36-45  
[18] Vílchez, J. M., & Pagel, B. E. J. 1988, MNRAS, 231, 257

## THE BOOKS

### In English

- [19] The properties of the ionized interstellar medium in spiral galaxies, Al-  
mudena Zurita Munoz 2001

### In Greek

- [20] Introduction in Astrophysics (Lesson' s notes), Vlachos Loukas

## THE WEB SITES

- [21] <http://www.ing.iac.es/>  
[22] [http://adsabs.harvard.edu/abstract\\_service.html](http://adsabs.harvard.edu/abstract_service.html)